# Methane Activation by Laser-Ablated V, Nb, and Ta Atoms: Formation of $CH_3-MH$, $CH_2=MH_2$, $CH\equiv MH_3^-$, and $(CH_3)_2MH_2$

**Han-Gook Cho and Lester Andrews***

*Department of Chemistry, University of Incheon, 177 Dohwa-dong, Nam-ku, Incheon 402-749, South Korea, and Department of Chemistry, University of Virginia, P.O. Box 400319, Charlottesville, Virginia 22904-4319*

*Received: December 2, 2005; In Final Form: January 25, 2006*

Methane activation by group 5 transition-metal atoms in excess argon and the matrix infrared spectra of reaction products have been investigated. Vanadium forms only the monohydrido methyl complex ($CH_3-VH$) in reaction with $CH_4$ and upon irradiation. On the other hand, the heavier metals form methyl hydride and methylidene dihydride complexes ($CH_3-MH$ and $CH_2=MH_2$) along with the methylidyne trihydride anion complexes ($CH\equiv MH_3^-$). The neutral products, particularly the methylidene complex, increase markedly on irradiation whereas the anionic product depletes upon UV irradiation or addition of a trace of $CCl_4$ or $CBr_4$ to trap electrons. Other absorptions that emerge on irradiation and annealing increase markedly at higher precursor concentration and are attributed to a higher-order product ($(CH_3)_2MH_2$). Spectroscopic evidence suggests that the agostic Nb and Ta methylidene dihydride complexes have two identical metal−hydrogen bonds.

## Introduction

Group 4−6 transition metals form alkylidene complexes that are important in synthetic chemistry.[1] Although tantalum derivatives were discovered first,[2,3] alkylidene chemistry is dominated by group 6, and stable group 4 alkylidene complexes are rare.[1] Naked group 4 metal atoms react with methane and methyl halides to produce simple methyl and methylidene complexes ($CH_3-MX$ and $CH_2=MHX$, X = H, F, Cl, Br, and I) along with a dimethyl complex ($(CH_3)_2MX_2$),[4−11] whereas group 6 transition metals form methyl, methylidene, and methylidyne hydride complexes ($CH_3-MX$, $CH_2=MHX$, and $CH\equiv MH_2X$).[12−15] Several of the products are photoreversible via α-hydrogen migration.[4,7,11,12−15] These simple methylidene and methylidyne complexes provide a basis to compare structures and substituent effects more easily than for much larger high-oxidation-state complexes. Such complexes are used for alkane activation and catalytic metathesis of alkenes, alkynes, and cyclic compounds, and they are typically generated by intramolecular α-hydrogen elimination from a bis(alkyl) precursor.[1,16,17] Large substituents are required to stabilize the electron-deficient metal center, and many of the complexes so formed are agostic. We have found greater reactivity for group 4 and 6 metal atoms with methyl fluoride than with methane, and the group 5 metal Nb reactions with $CH_3F$ gave analogous products starting with activation of the C−F bond.[18]

Density functional theory calculations using large basis sets show that the $CH_2$ group in the simple methylidene complexes ($CH_2=MHX$) is considerably distorted[4−15,18] and that the two metal−hydrogen bonds are not equivalent in the methylidene hydride complexes ($CH_2=MH_2$).[8−13] The effect of agostic distortion is identified accordingly in the infrared spectra of the methylidene dihydride complexes of groups 4 and 6 transition metals formed from $CH_2D_2$.[8−13] Earlier theoretical studies using minimum basis sets failed to characterize the agostic distortion,[19,20] and more recent multiconfiguration calculations fixed the $C_{2v}$ structure and found it to be stable.[21,22]

Group 5 transition metals have been important in the progress of coordination chemistry, forming various complexes with carbon−metal bonds.[1] Although vanadium produces complexes with CO and unsaturated hydrocarbons, it rarely forms high-oxidation-state complexes.[1] Niobium alkylidene complexes have been mostly synthesized via α-hydrogen abstraction reactions, and one-electron oxidation of a dibenzyl niobium (IV) complex led to a cationic Nb(V) benzylidene complex.[23] An anionic Nb methylidene complex was prepared by the unusual bimetallic cleavage of a carbon−oxygen bond. However, attempts to provide a Nb methylidyne complex have not been successful, leading to other related complexes instead.[1] In contrast, Ta has lead advances in the chemistry of high-oxidation-state complexes. Numerous Ta alkylidene complexes have been prepared, following the first preparation of $(\eta^5\text{-}C_5H_5)_2Ta(CH_2)(CH_3)$ and $(Me_3CCH_2)_3Ta(CHCMe_3)$ by α-hydrogen abstraction.[2] Several Ta alkylidyne complexes have been reported since the first Ta alkylidyne complexes synthesized by Schrock,[3,24] but Ta methylidyne complexes are not common. It is noteworthy that a $C_{3v}$ structure has been calculated for the simple $CH\equiv TaH_3^-$ anion complex.[21]

In this investigation, reactions of laser-ablated V, Nb, and Ta atoms with methane diluted in argon were carried out, and the products isolated in an argon matrix were investigated by means of infrared spectroscopy. Results indicate that only one C−H insertion reaction product is formed by vanadium, whereas four products including an anionic methylidyne hydride complex are identified for each heavier metal on the basis of the vibrational spectra and their variations upon photolysis, annealing, and the addition of a trace of $CCl_4$ or $CBr_4$ to trap ablated electrons. Unlike the previously studied methylidene dihydride complexes of groups 4 and 6 transition metals,[8−13] the agostic Nb and Ta methylidene hydride complexes appear to have structures with two identical metal−hydrogen bonds.

* To whom correspondence should be addressed. E-mail: lsa@virginia.edu.

10.1021/jp057029f CCC: $33.50 
Published on Web 02/28/2006

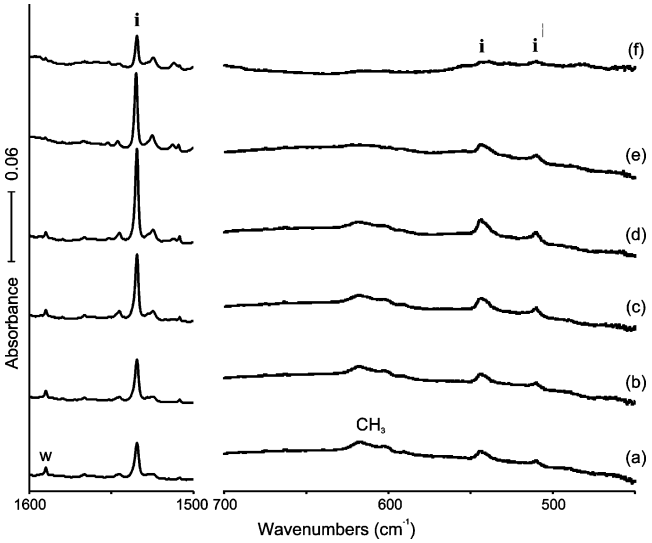


**Figure 1.** IR spectra in the regions of 1600−1500 and 700−450 $cm^{-1}$ for laser-ablated V atoms co-deposited with $CH_4$ in excess argon at 8 K. (a) V + 2% $CH_4$ in Ar co-deposited for 1 h. (b) After broad-band photolysis with a filter ($\lambda > 420$ nm) for 20 min. (c) After broad-band photolysis with a filter ($240 < \lambda < 380$ nm) for 20 min. (d) After broad-band photolysis with a filter ($\lambda > 220$ nm) for 20 min. (e) After annealing to 26 K. (f) After annealing to 34 K. Insertion product absorptions are marked **i**. The weak band labeled w is due to water impurity.

## Experimental and Computational Methods

Laser ablated group 5 metal atoms (Johnson-Matthey) were reacted with $CH_4$ (Matheson, UHP grade), $^{13}CH_4$, $CD_4$, and $CH_2D_2$ (Cambridge Isotopic Laboratories) in excess argon (MG Industries) during condensation on a CsI window at 8 K using methods previously described.[25−27] Concentrations of gas mixtures are typically 1−5% in argon. In addition, $CCl_4$ (0.04−0.2%) or $CBr_4$ (0.1%) was included in the gas mixture to capture electrons produced in the laser-ablation process in complimentary experiments.[26] After reaction, infrared spectra were recorded at a resolution of 0.5 $cm^{-1}$ using a Nicolet 550 spectrometer with an HgCdTe type-B detector. Samples were then irradiated by a mercury arc lamp (175 W, globe removed) using a combination of optical filters, were annealed, and more spectra were recorded.

Complementary density functional theory (DFT) calculations were carried out using the Gaussian 03 package,[28] B3LYP density functional, 6-311++G(3df,3pd) basis sets for C, H, V and SDD pseudopotential and basis set for Nb and Ta to provide a consistent set of vibrational frequencies for the reaction products. BPW91, MP2, or CCSD calculations were done to compliment the B3LYP results. Geometries were fully relaxed during optimization, and the optimized geometry was confirmed by vibrational analysis. All the vibrational frequencies were calculated analytically. In calculation of the binding energy of a metal complex, the zero-point energy is included.

## Results

Reactions of V, Nb, and Ta atoms with methane isotopomers were carried out, and the observed vibrational characteristics of the products are compared with the calculated results.

**V + $CH_4$.** Vanadium is very reactive with $CH_4$, probably one of the most reactive among group 4−6 transition metals. The spectra observed from the V + $CH_4$ reaction products are shown in Figure 1. Although the spectra are relatively simple, a very strong product absorption is observed at 1534.4 $cm^{-1}$ (marked **i**). The absorption grows about 20% upon visible (hereafter "visible" denotes ">420 nm") photolysis, almost doubles upon following near UV (hereafter "near UV" denotes "240−380 nm") photolysis, and grows another 100% upon full arc (hereafter full arc denotes ">220 nm") irradiation. These irradiations increase the absorption at 1534.4 $cm^{-1}$ and associated (Figure 1d) absorptions at 541.6 and 510.1 $cm^{-1}$.

**TABLE 1: Observed and Calculated Fundamental Frequencies of $CH_3$−VH Isotopomers in the Ground $^4A''$ Electronic State[a]**

| approximate description | $CH_3$−VH freq obs | $CH_3$−VH freq calc | $CH_3$−VH int | $CD_3$−VD freq obs | $CD_3$−VD freq calc | $CD_3$−VD int |
|---|---|---|---|---|---|---|
| A′ $CH_3$ str | | 3066.7 | 11 | | 2268.1 | 4 |
| A′ $CH_3$ str | | 2987.6 | 7 | | 2139.1 | 2 |
| A′ V−H str | 1534.4 | 1631.5 | 336 | 1106.5 | 1166.1 | 177 |
| A′ $CH_3$ scis | | 1423.3 | 1 | | 1033.2 | 1 |
| A′ $CH_3$ deform | | 1129.4 | 0 | | 887.5 | 6 |
| A′ CVH bend | 543.8 | 560.5 | 105 | 464.7 | 456.8 | 79.2 |
| A′ C−V str | 510.1 | 487.2 | 41 | 453.6 | 412.3 | 12 |
| A′ $CH_3$ rock | | 332.9 | 47 | | 238.2 | 26 |
| A″ $CH_3$ str | | 3069.2 | 25 | | 2268.1 | 10 |
| A″ $CH_3$ scis | | 1419.8 | 3 | | 1030.9 | 3 |
| A″ $CH_2$ twist | | 383.3 | 1 | | 284.7 | 2 |
| A″ $CH_3$ distort | | 91.5 | 59 | | 67.1 | 32.8 |

[a] B3LYP/6-311++G(3df,3pd) level. Frequencies and intensities are in $cm^{-1}$ and km/mol. Infrared intensities are calculated values.

Deuteration causes a shift by a larger factor in the hydrogen stretching than the lower frequency region. A strong absorption at 1106.5 $cm^{-1}$ and a weak absorption at 464.7 $cm^{-1}$ show the same changes in intensity on irradiation and annealing. Table 1 collects the observed frequencies. The $CH_3$ and $CD_3$ radicals are also observed in our spectra.[9−13,29]

**Nb + $CH_4$.** In the case of Nb + $CH_4$, four different sets of product absorptions are observed on the basis of the variation in intensity upon photolysis, annealing, and the addition of $CCl_4$. The spectra from Nb + $CH_4$ reaction are shown in Figure 2. In the Nb−H stretching region (1750−1450 $cm^{-1}$), strong diagnostic product absorptions are observed with about 1:2 intensity ratio at 1680.7 and 1652.5 $cm^{-1}$ (marked **m**) in the spectra. They are found even in the spectrum with a trace of $CCl_4$ (Figure 3a, after visible photolysis following deposition). These bands show dramatic (more than 300%) and slight (30%) increases in intensity upon visible and near UV photolysis, respectively, and increase another 100% upon full-arc irradiation. They sharpen but show only a slight decrease in intensity on annealing up to 26 K. Three additional absorptions at 805.4, 547.1, and 480.4 $cm^{-1}$ show the same intensity variation, particularly the dramatic increase in intensity upon visible photolysis.

Below the **m** absorptions in the Nb−H stretching region, a weak absorption marked **i** is observed at 1611.4 $cm^{-1}$ in the water residue absorption region. This absorption increases moderately in the process of photolysis, and gradually decreases upon annealing while neighboring water absorptions decrease.

On the lower frequency side of the Nb−H stretching region, below $NbH_2$ at 1569.1 $cm^{-1}$ and NbH at 1555.9 $cm^{-1}$,[30] two absorptions are observed at 1542.5 and 1489.5 $cm^{-1}$ (marked **a**), which remain almost unchanged upon visible and near UV photolysis but decrease substantially upon full-arc irradiation and annealing. A more dramatic change in intensity occurs in the spectrum with trace of $CCl_4$, where the two absorptions vanish while other absorptions are still evident

Above the **m** absorptions in the Nb−H stretching region, new absorptions are observed at 1717.5 and 1686.3 $cm^{-1}$ marked **di**. These absorptions are weak in the original spectrum after

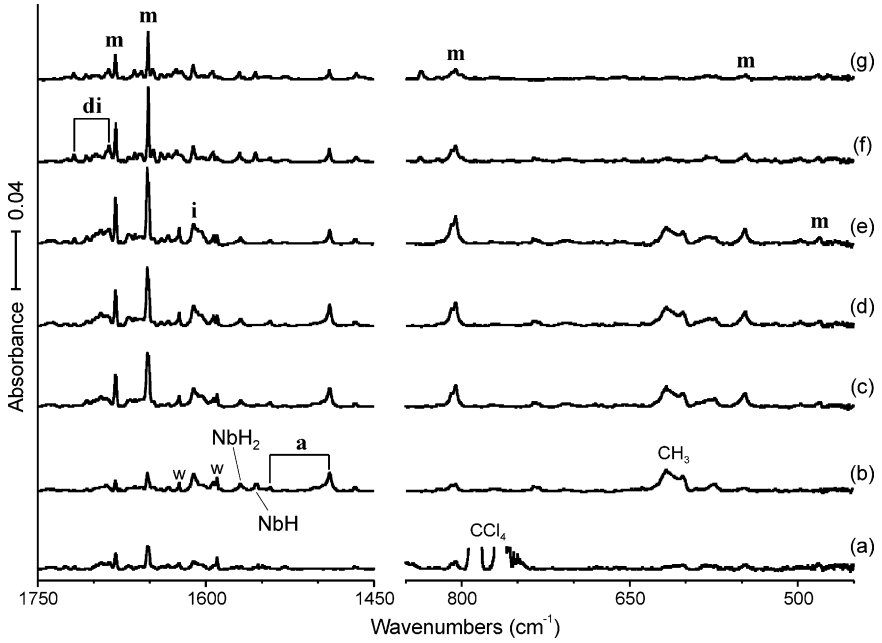


**Figure 2.** IR spectra in the regions of 1750−1450 and 850−450 $cm^{-1}$ for laser-ablated Nb atoms co-deposited with $CH_4$ in excess argon at 8 K. (a) After broad-band photolysis with a filter ($\lambda$ > 420 nm) following co-deposition of Nb + [2% $CH_4$ + 0.04% $CCl_4$] in Ar for 1 h. (b) Nb + 2% $CH_4$ in Ar co-deposited for 1 h. (c) After broad-band photolysis with a filter ($\lambda$ > 420 nm) for 20 min. (d) After broad-band photolysis with a filter (240 < $\lambda$ < 380 nm) for 20 min. (e) After broad-band photolysis with a filter ($\lambda$ > 220 nm) for 20 min. (f) After annealing to 26 K. (g) After annealing to 32 K. **m**, **i**, **a**, and **di** stand for the product absorption groups.

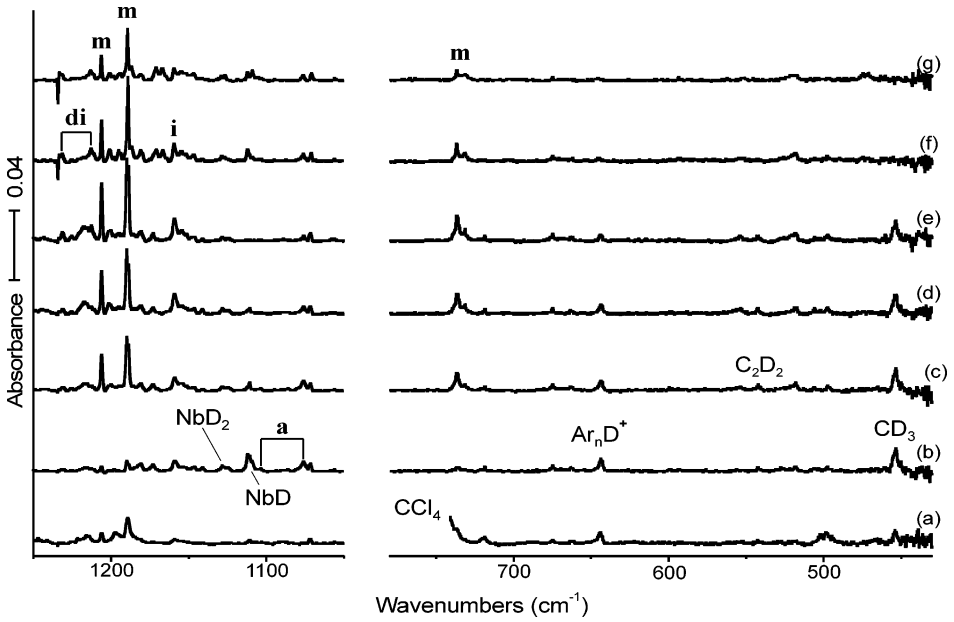


**Figure 3.** IR spectra in the regions of 1250−1050 and 780−430 $cm^{-1}$ for laser-ablated Nb atoms co-deposited with $CD_4$ in excess argon at 8 K. (a) After broad-band photolysis with a filter ($\lambda$ > 420 nm) following co-deposition of Nb + [2% $CD_4$ + 0.1% $CCl_4$] in Ar for 1 h. (b) Nb + 2% $CD_4$ in Ar co-deposited for 1 h. (c) After broad-band photolysis with a filter ($\lambda$ > 420 nm) for 20 min. (d) After broad-band photolysis with a filter (240 < $\lambda$ < 380 nm) for 20 min. (e) After broad-band photolysis with a filter ($\lambda$ > 220 nm) for 20 min. (f) After annealing to 26 K. (g) After annealing to 32 K. **m**, **i**, **a**, and **di** stand for the product absorption groups.

deposition, but they increase on full-arc irradiation and sharpen on annealing.

Isotopic substitution of the methane precursor provides essential information. The product absorptions of Nb + $CH_4$ isotopomers observed in this study are listed in Table 2 and compared with calculated values for possible product molecules in Tables 3−6. Parts a and b of Table 3 report frequencies calculated for two different low-energy structural configurations of the $CH_2{=}NbH_2$ product complex. The $^{13}C$ substitution has no significant effect on the absorptions in the hydrogen stretching frequency region, but small shifts are observed in the low-frequency region. All bands are shifted with $CD_4$ by larger factors in the upper than in the lower frequency region.

In Figure 3 (Nb + $CD_4$), two strong absorptions marked **m** are observed at 1206.0 and 1189.9 $cm^{-1}$ and another one at 736.8 $cm^{-1}$. They are also evident in the spectrum with trace of $CCl_4$ (after visible photolysis following deposition). Though similar, they show larger variation in intensity on irradiation than in the case of Nb + $CH_4$. Also shown in Figure 3 is the **i** absorption the at 1159.1 $cm^{-1}$.

Two absorptions marked **a** are observed at 1103.7 and 1076.1 $cm^{-1}$. They decrease slightly and more substantially upon near

**TABLE 2: Frequencies of Product Absorptions Observed from Reactions of Methane with Nb in Excess Argon[a]**

| group | $CH_4$ | $CD_4$ | $^{13}CH_4$ | $CH_2D_2$ | description |
|---|---|---|---|---|---|
| **i** | **1611.4**, 1608.3 | 1159.1 | 1611.4 | 1611.0, **1608.2** | Nb−H str |
| **m** | 1680.7, 1680.0 (sh) | 1206.0, 1205.8 (sh) | 1680.7, 1680.1 (sh) | 1680.7, **1666.4**, 1652.5 | $NbH_2$ sym str |
| | **1652.5**, 1651.0 | **1189.9**, 1188.7 | **1652.5**, 1650.9 | 1205.5, **1198.4**, 1188.7 | $NbH_2$ antisym str |
| | 805.4 | 736.8 | 784.5 | | C═Nb str |
| | 547.1 | | 546.6 | | $CH_2$ wag |
| | 480.4 | | 480.4 | | $NbH_2$ rock |
| **a** | 1542.5 | 1103.7 | 1542.2 | 1524.3 | $NbH_3$ sym str |
| | 1489.5 | 1076.1 | 1489.5 | 1506.7, 1488.2 | $NbH_3$ antisym str |
| **di** | 1717.5 | 1231.5 | 1717.5 | 1717.1, 1707.9, **1694.5, 1686.3** | $NbH_2$ sym str |
| | 1686.3 | 1213.0 | 1686.3 | 1217.8, 1212.8 | $NbH_2$ antisym str |

[a] All frequencies are in $cm^{-1}$. Stronger absorptions are bold. Description gives major coordinate.

**TABLE 3: Observed and Calculated Fundamental Frequencies of $CH_2$═$NbH_2$ Isotopomers**

(a) Configuration 1 in the $C_1$ Symmetry Ground $^2A$ Electronic State[a]

| | $CH_2$═$NbH_2$ | | | | | $CD_2$═$NbD_2$ | | | | | $^{13}CH_2$═$NbH_2$ | | | | |
|---|---|---|---|---|---|---|---|---|---|---|---|---|---|---|---|
| | | BPW91 | | B3LYP | | | BPW91 | | B3LYP | | | BPW91 | | B3LYP | |
| approximate description | obs | freq | int | freq | int | obs | freq | int | freq | int | obs | freq | int | freq | int |
| A′ $CH_2$ str | | 3156.5 | 6 | 3183.2 | 1 | | 2237.8 | 9 | 2357.4 | 3 | | 3145.7 | 6 | 3172.1 | 1 |
| A′ C−H str | | 2537.6 | 2 | 2941.0 | 2 | | 1847.1 | 2 | 2138.3 | 3 | | 2531.8 | 2 | 2934.4 | 2 |
| A′ $NbH_2$ str | 1680.7 | 1745.6 | 147 | 1748.9 | 234 | 1206.0 | 1240.1 | 125 | 1242.6 | 150 | 1680.7 | 1745.6 | 146 | 1748.9 | 234 |
| A′ $NbH_2$ str | 1652.5 | 1736.8 | 335 | 1734.2 | 482 | 1189.9 | 1237.8 | 122 | 1235.2 | 219 | 1652.5 | 1736.8 | 336 | 1734.2 | 482 |
| A′ $CH_2$ scis | | 1364.4 | 26 | 1301.2 | 12 | | 1037.6 | 17 | 1030.4 | 20 | | 1358.6 | 26 | 1291.3 | 11 |
| A′ C═Nb str | 805.4 | 849.5 | 70 | 806.0 | 94 | 736.8 | 763.1 | 45 | 687.2 | 44 | 784.5 | 827.6 | 70 | 795.6 | 93 |
| A′ $NbH_2$ scis | | 722.0 | 7 | 732.9 | 4 | | 553.9 | 2 | 544.7 | 10 | | 717.1 | 7 | 723.4 | 4 |
| A′ $CH_2$ wag | 547.1 | 608.6 | 75 | 672.5 | 119 | | 461.5 | 60 | 521.4 | 82 | 546.6 | 603.7 | 71 | 667.0 | 116 |
| A′ $NbH_2$ rock | | 656.8 | 36 | 584.3 | 5 | | 493.6 | 6 | 442.6 | 3 | | 654.6 | 39 | 581.1 | 5 |
| A″ $CH_2$ twist | 480.4 | 487.3 | 75 | 337.2 | 10 | | 348.2 | 39 | 241.1 | 5 | 480.4 | 487.0 | 74 | 336.9 | 10 |
| A″ $CH_2$ rock | | 529.3 | 44 | 234.8 | 28 | | 377.8 | 24 | 169.2 | 14 | | 528.7 | 44 | 234.4 | 29 |
| A″ $NbH_2$ twist | | 198.2 | 24 | 167.0 | 115 | | 140.7 | 12 | 121.8 | 59 | | 198.2 | 24 | 166.8 | 115 |

(b) Configuration 2 in the $C_s$ Symmetry Ground $^2A'$ Electronic State[b]

| | $CH_2$═$NbH_2$ | | | $CD_2$═$NbD_2$ | | | $^{13}CH_2$═$NbH_2$ | | | CHD═NbHD | | |
|---|---|---|---|---|---|---|---|---|---|---|---|---|
| | freq | | | freq | | | freq | | | freq | | |
| approximate description | obs | calc | int | obs | calc | int | obs | calc | int | obs | calc | int |
| A′ C−H str | | 3162.9 | 7 | | 2342.8 | 10 | | 3152.1 | 7 | | 2486.9 | 15 |
| A′ C−H str | | 2462.2 | 16 | | 1792.0 | 6 | | 2456.6 | 17 | | 2314.1 | 10 |
| A′ Nb−H str | 1680.7 | 1750.5 | 157 | 1206.0 | 1242.6 | 79 | 1680.7 | 1750.4 | 157 | 1666.4 | 1747.4 | 232 |
| A′ $CH_2$ scis | | 1349.2 | 27 | | 1033.7 | 16 | | 1342.8 | 27 | | 1260.8 | 25 |
| A′ C═Nb str | 805.4 | 852.3 | 66 | 736.8 | 762.5 | 46 | 784.5 | 830.0 | 65 | 805.4 | 810.8 | 53 |
| A′ $NbH_2$ scis | | 677.7 | 78 | | 492.3 | 16 | | 677.3 | 78 | | 589.4 | 60 |
| A′ $NbH_2$ wag | | 621.0 | 32 | | 486.6 | 40 | | 615.1 | 32 | | 538.8 | 26 |
| A′ $CH_2$ rock | 547.1 | 545.3 | 57 | | 390.5 | 27 | 546.6 | 544.9 | 57 | | 466.6 | 28 |
| A″ Nb−H str | 1652.5 | 1744.8 | 311 | 1189.9 | 1245.2 | 161 | 1652.5 | 1744.8 | 311 | 1198.4 | 1243.8 | 114 |
| A″ $CH_2$ wag | | 582.9 | 10 | | 444.5 | 9 | | 578.8 | 8 | | 495.4 | 29 |
| A″ $NbH_2$ twist | 480.4 | 471.8 | 69 | | 336.8 | 36 | 480.4 | 471.5 | 68 | | 359.3 | 34 |
| A″ $CH_2$ twist | | 310.8 | 6 | | 220.7 | 3 | | 310.7 | 6 | | 286.6 | 8 |

[a] B3LYP and BPW91/6-311++G(3df,3pd)/SDD levels. Frequencies and intensities are in $cm^{-1}$ and km/mol. Infrared intensities are calculated values. [b] BPW91/6-311++G(3df,3pd)/SDD level. Frequencies and intensities are in $cm^{-1}$ and km/mol. Infrared intensities are calculated values.

UV and full arc irradiation, respectively, and later slightly recover in the early stage of annealing and decrease at higher temperature. Analogous to the $CH_4$ counterparts, their frequencies are lower than the deuterium stretching frequencies of deuterated niobium hydrides (1128.5 $cm^{-1}$ for $NbD_2$ and 1112.2 $cm^{-1}$ for NbD).[30] Addition of a trace of $CCl_4$ completely depletes the absorptions (Figure 3a). On the blue side of the **m** absorptions in the Nb−D stretching region, the two absorptions marked **di** at 1231.5 and 1213.0 $cm^{-1}$ become apparent in the process of photolysis and grow further on the early stage of annealing.

$CH_2D_2$ provides additional diagnostic absorptions in the Nb−H and Nb−D stretching regions (Figure 4). Two strong absorptions marked **m** appear at 1666.4 and 1198.4 $cm^{-1}$, each at the middle of the metal−hydrogen or metal-deuterium stretching absorption pair, suggesting that the product responsible for **m** absorptions in fact contains two identical metal−hydrogen bonds. Both absorptions increase dramatically upon visible, near UV, and full arc irradiation, respectively (1000% in total!). The three absorptions at 1524.3, 1506.7, and 1488.2 $cm^{-1}$ (marked **a**) decrease substantially upon full arc irradiation and recover slightly in the early stage of annealing.

At higher concentrations of the precursor, the absorptions marked **di** become much stronger relative to the other three sets of product absorptions. The Nb−H and Nb−D stretching regions (after annealing to 26 K) at high (5%) concentration of the precursor are compared with those at lower concentration (2%), as shown in Figure 5. The intensity ratio between the higher and lower frequency components of a pair is about 1:2. The **di** absorptions also increase in the process of photolysis and slightly

**TABLE 4: Observed and Calculated Fundamental Frequencies of $CH_3-NbH$ Isotopomers in the Ground $^4A''$ Electronic State[a]**

| approximate description | $CH_3-NbH$ | | | $CD_3-Nb-D$ | | | $^{13}CH_3-NbH$ | | | $CHD_2-NbH$ | | | $CH_2D-NbD$ | | |
|---|---|---|---|---|---|---|---|---|---|---|---|---|---|---|---|
| | freq | | | freq | | | freq | | | freq | | | freq | | |
| | obs | calc | int | obs | calc | int | obs | calc | int | obs | calc | int | obs | calc | int |
| A′ $CH_3$ str | | 3057.3 | 8 | | 2262.0 | 3 | | 3046.4 | 9 | | 3028.1 | 11 | | 3009.7 | 1 |
| A′ $CH_3$ str | | 2975.9 | 3 | | 2130.8 | 1 | | 2973.2 | 3 | | 2176.1 | 0 | | 2212.4 | 4 |
| A′ Nb−H str | 1611.4 | 1706.3 | 314 | 1159.1 | 1213.9 | 161 | 1611.4 | 1706.3 | 314 | 1611.0 | 1706.2 | 314 | *b* | 1213.9 | 161 |
| A′ $CH_3$ scis | | 1410.8 | 2 | | 1024.4 | 1 | | 1407.6 | 2 | | 1118.0 | 1 | | 1379.9 | 2 |
| A′ $CH_3$ deform | | 1151.1 | 3 | | 908.2 | 14 | | 1141.2 | 2 | | 952.2 | 10 | | 1072.0 | 4 |
| A′ CNbH bend | | 596.7 | 52 | | 437.9 | 8 | | 593.4 | 52 | | 563.7 | 31 | | 438.6 | 6 |
| A′ C−Nb str | | 497.8 | 54 | | 458.0 | 57 | | 485.4 | 53 | | 480.4 | 76 | | 513.8 | 66 |
| A′ $CH_3$ rock | | 353.6 | 20 | | 252.8 | 12 | | 353.1 | 19 | | 315.4 | 10 | | 267.6 | 17 |
| A″ $CH_3$ str | | 3055.0 | 6 | | 2256.9 | 2 | | 3044.4 | 6 | | 2256.9 | 2 | | 3054.6 | 6 |
| A″ $CH_3$ scis | | 1410.6 | 4 | | 1024.4 | 3 | | 1407.3 | 4 | | 1261.3 | 5 | | 1207.0 | 3 |
| A″ $CH_2$ twist | | 352.0 | 0 | | 259.9 | 0 | | 350.6 | 0 | | 272.0 | 1 | | 334.7 | 2 |
| A″ $CH_3$ distort | | 151.2 | 33 | | 108.7 | 18 | | 151.0 | 33 | | 141.6 | 38 | | 116.9 | 14 |

[a] B3LYP/6-311++G(3df,3pd)/SDD level. Frequencies and intensities are in $cm^{-1}$ and km/mol. Infrared intensities are calculated values. [b] Overlapped by precursor absorption.

**TABLE 5: Observed and Calculated Fundamental Frequencies of $CH{\equiv}NbH_3^-$ Isotopomers in the Ground $^1A_1$ Electronic State[a]**

| approximate description | $CH{\equiv}NbH_3^-$ | | | $CD{\equiv}NbD_3^-$ | | | $^{13}CH{\equiv}NbH_3^-$ | | | $CH{\equiv}NbHD_2^-$ | | | $CD{\equiv}NbDH_2^-$ | | |
|---|---|---|---|---|---|---|---|---|---|---|---|---|---|---|---|
| | freq | | | freq | | | freq | | | freq | | | freq | | |
| | obs | calc[b] | int | obs | calc[b] | int | obs | calc[b] | int | obs | calc[b] | int | obs | calc[b] | int |
| $A_1$ C−H str | | 3121.0 | 13 | | 2314.4 | 8 | | 3110.0 | 15 | | 3121.0 | 13 | | 2314.5 | 0 |
| $A_1$ $NbH_3$ str | 1542.5 | 1593.3 | 381 | 1103.7 | 1129.1 | 168 | 1542.2 | 1593.1 | 383 | *b* | 1120.2 | 255 | 1524.3 | 1575.8 | 500 |
| $A_1$ C≡Nb str | | 955.0 | 188 | | 910.6 | 161 | | 926.7 | 181 | | 950.8 | 183 | | 914.9 | 173 |
| $A_1$ $NbH_3$ deform | | 608.1 | 119 | | 437.5 | 62 | | 607.1 | 116 | | 545.0 | 140 | | 560.6 | 92 |
| E $NbH_3$ str | 1489.5 | 1540.1 | 778 × 2 | 1076.1 | 1101.4 | 401 × 2 | 1489.5 | 1540.0 | 777 × 2 | 1506.7 | 1557.8 | 620 | 1488.2 | 1539.1 | 759 |
| | | | | | | | | | | *b* | 1103.1 | 425 | *b* | 1111.4 | 351 |
| E $NbH_3$ scis | | 618.0 | 105 × 2 | | 466.3 | 9 × 2 | | 617.3 | 116 × 2 | | 542.7 | 81 | | 614.1 | 123 |
| | | | | | | | | | | | 438.7 | 70 | | 559.1 | 45 |
| E NbCH bend | | 581.6 | 111 × 2 | | 433.5 | 104 × 2 | | 576.7 | 99 × 2 | | 588.9 | 29 | | 473.4 | 99 |
| | | | | | | | | | | | 573.9 | 91 | | 462.6 | 38 |
| E $NbH_3$ rock | | 455.1 | 8 × 2 | | 326.4 | 7 × 2 | | 454.8 | 8 × 2 | | 368.7 | 5 | | 387.1 | 16 |
| | | | | | | | | | | | 357.3 | 6 | | 348.0 | 23 |

[a] B3LYP/6-311++G(3df,3pd)/SDD level. Frequencies and intensities are in $cm^{-1}$ and km/mol. Infrared intensities are calculated values. [b] Overlapped by precursor absorption.

**TABLE 6: Observed and Calculated Strongest Frequencies of $(CH_3)_2NbH_2$ Isotopomers in the Ground $^2A_2$ Electronic State[a]**

| approximate description | $(CH_3)_2NbH_2$ | | | $(CD_3)_2NbD_2$ | | | $(^{13}CH_3)_2NbH_2$ | | | $(C_2H_3D_3)NbHD$ | | |
|---|---|---|---|---|---|---|---|---|---|---|---|---|
| | freq | | | freq | | | freq | | | freq | | |
| | obs | calc | int | obs | calc | int | obs | calc | int | obs | calc | int |
| $\nu_3$ $A_1$ $NbH_2$ str | 1717.5 | 1777.2 | 276 | 1231.5 | 1261.2 | 143 | 1717.5 | 1777.2 | 276 | 1707.9, 1694.5 | 1764.3 | 334 |
| $\nu_{16}$ $B_1$ $NbH_2$ str | 1686.3 | 1751.4 | 397 | 1213.0 | 1249.3 | 206 | 1686.3 | 1751.4 | 397 | *b*, 1217.8 | 1255.5 | 177 |
| $\nu_6$ $A_1$ $NbH_2$ scis | | 650.0 | 109 | | 520.1 | 46 | | 648.9 | 106 | | 581.7 | 96 |
| $\nu_{26}$ $B_2$ $NbH_2$ wag | | 495.9 | 178 | | 376.0 | 60 | | 492.4 | 190 | | 484.2 | 124.2 |

[a] B3LYP/6-311++G(3df,3pd)/SDD level. Frequencies and infrared intensities are in $cm^{-1}$ and km/mol. Infrared intensities are calculated values. [b] Overlapped by precursor absorption.

in the early stage of annealing as shown in Figures 2−5. The increases in intensity at higher concentration indicate that the **di** absorptions most likely arise from a higher-order methane reaction product.

**Ta + $CH_4$.** Parallel to the niobium system, four sets of product absorptions are observed, and the spectra from Ta + $CH_4$ reaction products are shown in Figure 6. Two product absorptions marked **m** with about 1:2 intensity ratio are observed at 1753.8 and 1731.9 $cm^{-1}$ in the Ta−H stretching region, which are compared with frequencies of 1758.9 and 1732.9 $cm^{-1}$ of $TaH_2$.[30] The binary tantalum hydride absorptions are not observed in this study, as the strongest $TaH_2$ band would be masked by the strongest **m** band. The new **m** bands show substantial increases in intensity upon visible, near UV, and full arc irradiation, respectively, and decrease gradually on annealing. Two more **m** absorptions are observed at 825.6 and 637.7 $cm^{-1}$.

On red side, a product absorption marked **i** is observed at 1726.2 $cm^{-1}$, which shows negligible intensity variation upon visible photolysis but increases about 70 and 60% (130% in total) upon near UV and full arc irradiation, respectively. It decreases completely upon annealing. On the lower frequency side of the Ta−H stretching region, a strong product absorption marked **a** is observed at 1567.8 $cm^{-1}$ (the weaker, higher frequency component is probably overlapped by the water residue absorptions). The absorption increases slightly upon visible irradiation but decreases upon near UV and full arc irradiation. It increases slightly in the early stage of annealing and later gradually decreases. More importantly, the absorption is not observed in the presence of a trace (0.1%) of $CBr_4$. In the low-frequency region in Figure 6, two associated absorptions are observed at 917.6 and 574.6 $cm^{-1}$. On the blue side of the **m** absorptions in the hydrogen stretching frequency region, two product absorptions marked **di** are observed at 1787.8 and

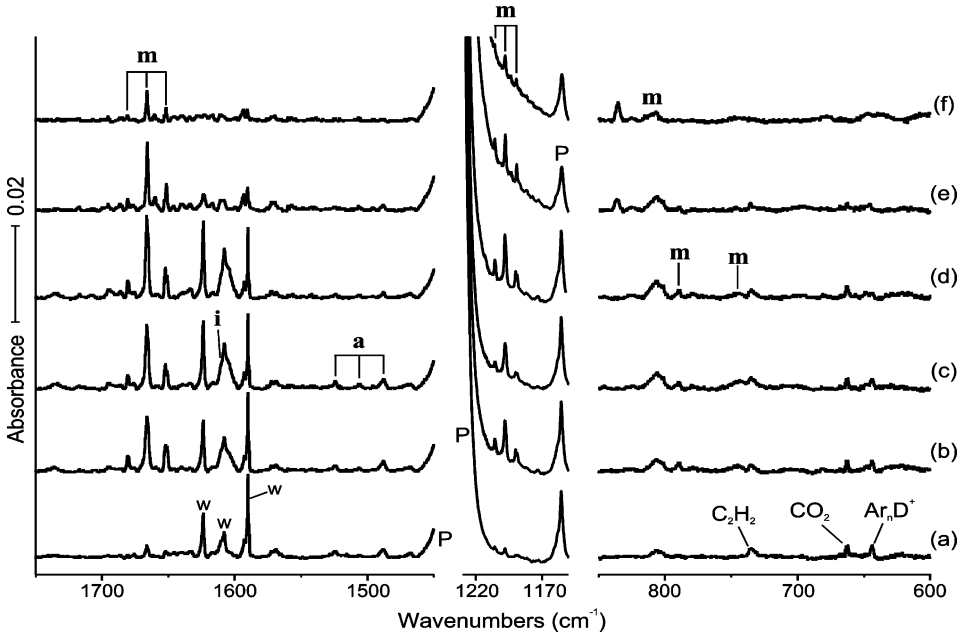


**Figure 4.** IR spectra in the regions of 1750−1450, 1230−1050, and 850−600 $cm^{-1}$ for laser-ablated Nb atoms co-deposited with $CH_2D_2$ in excess argon at 8 K. (a) Nb + 2% $CH_2D_2$ in Ar co-deposited for 1 h. (b) After broad-band photolysis with a filter ($\lambda > 420$ nm) for 20 min. (c) After broad-band photolysis with a filter ($240 < \lambda < 380$ nm) for 20 min. (d) After broad-band photolysis with a filter ($\lambda > 220$ nm) for 20 min. (e) After annealing to 26 K. (f) After annealing to 32 K. **m**, **i**, **a**, and **di** stand for the product absorption groups. "P" and "w" denote the precursor and water residue absorptions, respectively.

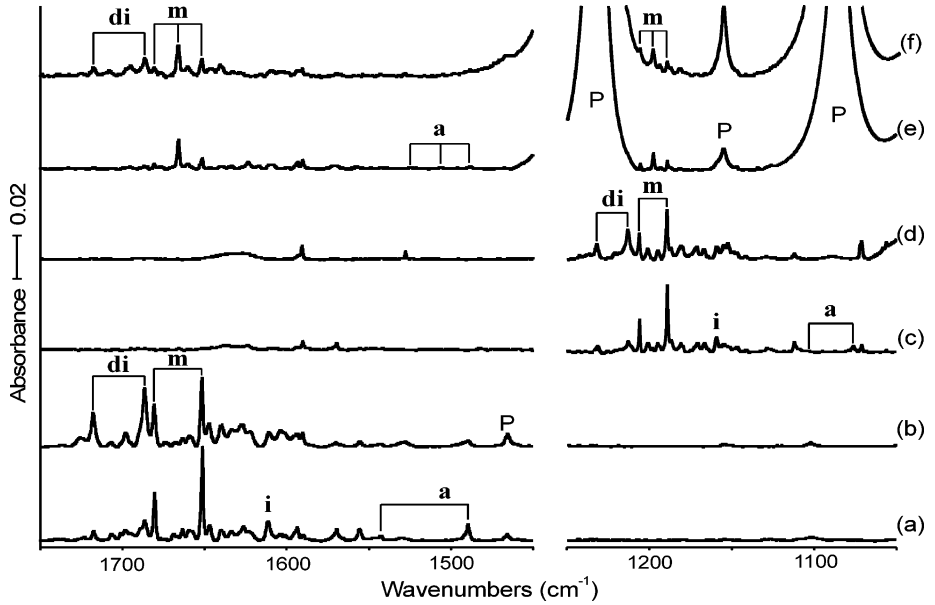


**Figure 5.** IR spectra in the regions of 1750−1450 and 1250−1150 $cm^{-1}$ for laser-ablated Nb atoms after annealing to 26 K following co-deposition of Nb atoms with $CH_4$ isotopomers in excess argon at 8 K for 1 h: (a) 2% $CH_4$; (b) 5% $CH_4$; (c) 2% $CD_4$; (d) 5% $CD_4$; (e) 2% $CH_2D_2$; (f) 5% $CH_2D_2$. **m**, **i**, **a**, and **di** stand for the product absorption groups. "P" denotes the precursor absorption.

1761.4 $cm^{-1}$. They increase on visible, near UV, and full arc irradiation and decrease upon annealing.

Reactions with isotopic precursors ($^{13}CH_4$, $CD_4$, $CH_2D_2$) provide essential information, and the measured frequencies of the isotopomer product absorptions are listed in Table 7 and compared with the calculated values in Tables 8−11. The $^{13}C$ substitution has negligible effect on the bands in the hydrogen stretching frequency region, but small shifts are observed in the low-frequency region. All bands are shifted with $CD_4$ by larger factors in the Ta−D stretching than the lower frequency region. Figure 7 shows the observed spectra from Ta + $CD_4$ reaction. Two **m** absorptions are observed at 1255.6 and 1243.6 $cm^{-1}$ in the Ta−D stretching region, which are compared with 1260.8 and 1244.1 $cm^{-1}$ of $TaD_2$.[30b] The other product absorptions are indicated.

$CH_2D_2$ provides further diagnostic information. Parallel to the case of Nb + $CH_4$, two strong absorptions marked **m** appear at 1742.5 and 1249.8 $cm^{-1}$ in Figure 8, each at the middle of the metal−hydrogen stretching absorption pair. They suggest that the product responsible for **m** absorptions contains two identical metal−hydrogen bonds. On the high-frequency side in the hydrogen stretching region, absorptions marked **di** are observed at 1774.5 and 1269.0 $cm^{-1}$, each at the middle of the **di** hydrogen stretching absorption pair. The **di** absorptions become much stronger at higher concentration of the precursor. Shown in Figure 9 are the spectra with 2 and 5% methane

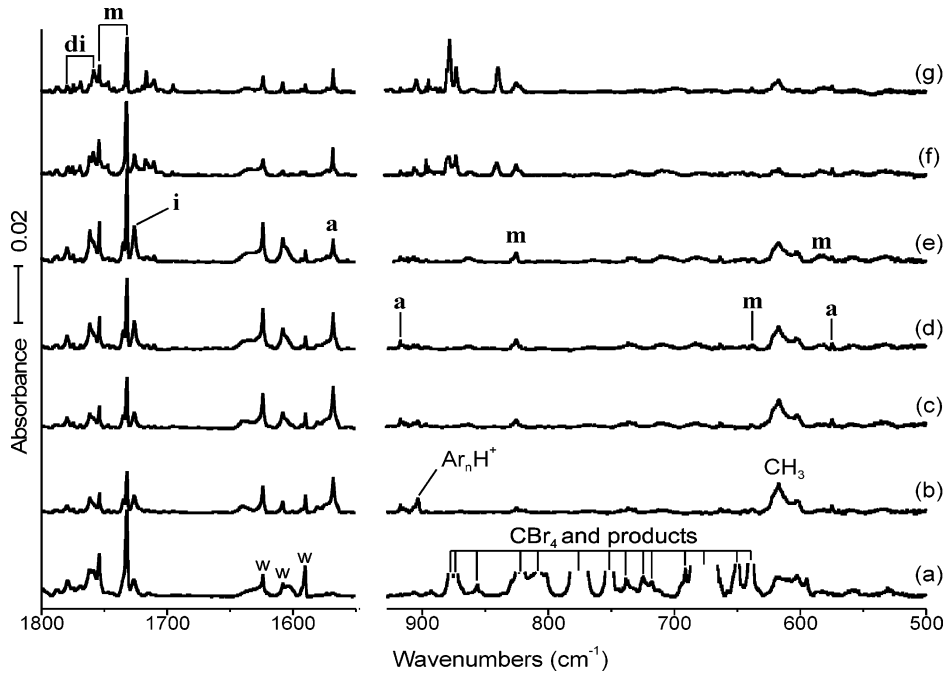


**Figure 6.** IR spectra in the regions of 1800−1550 and 930−500 $cm^{-1}$ for laser-ablated Ta atoms co-deposited with $CH_4$ in excess argon at 8 K. (a) After broad-band photolysis with a filter ($\lambda$ > 420 nm) following co-deposition of Ta + [1% $CH_4$ + 0.1% $CBr_4$] in Ar for 1 h. (b) Ta + 1% $CH_4$ in Ar co-deposited for 1 h. (c) After broad-band photolysis with a filter ($\lambda$ > 420 nm) for 20 min. (d) After broad-band photolysis with a filter (240 < $\lambda$ < 380 nm) for 20 min. (e) After broad-band photolysis with a filter ($\lambda$ > 220 nm) for 20 min. (f) After annealing to 26 K. (g) After annealing to 32 K. **m**, **i**, **a**, and **di** indicate the product absorption groups, and w denotes water residue absorptions.

**TABLE 7: Frequencies of Product Absorptions Observed from Reactions of Methane with Ta in Excess Argon**[a]

| group | $CH_4$ | $CD_4$ | $^{13}CH_4$ | $CH_2D_2$ | description |
|---|---|---|---|---|---|
| **i** | 1726.2 | 1236.8 | 1726.0 | 1724.6 | Ta−H str |
| **m** | 1753.8 | 1255.6 | 1753.8 | 1754.1, 1742.5, 1732.1 | $TaH_2$ sym str |
| | 1731.9 | 1243.6 | 1731.9 | 1255.9, 1249.8 | $TaH_2$ antisym str |
| | 825.6 | 740.0 | 803.4 | 780.0 | C═Ta str |
| | 637.7 | 522.5(?) | | | $TaH_2$ scis (?) |
| | 584.9 | | | | $CH_2$ wag (?) |
| **a** | | 1160.9 | | 1604.6, 1585.2, 1566.0, | $A_1$ $TaH_3$ str |
| | 1567.8 | 1126.6 | 1567.7 | 1150.2, 1139.4, 1128.6 | E $TaH_3$ str |
| | 917.6 | 862.8 | 889.0 | 916.1 | C≡Ta str |
| | 574.6 | | 569.7 | | E TaCH bend |
| **di** | 1787.8 | 1275.4 | 1787.8 | 1787, 1772, 1758 | $TaH_2$ sym str |
| | 1761.4 | 1260.3 | 1761.4 | 1270, 1261 | $TaH_2$ antisym str |

[a] All frequencies are in $cm^{-1}$. Description gives major coordinate.

isotopomers after annealing to 26 K. Clearly the **di** absorptions become much stronger at higher precursor concentration relative to the other sets of product absorptions, indicating the **di** absorptions arise from a higher-order reaction product.

## Discussion

The group 5 metal methane activation products will be considered for each metal in turn.

**V + $CH_4$.** The relatively simple spectrum (Figure 1) suggests that only one reaction product is formed with vanadium. The single strong product absorption at 1534.4 $cm^{-1}$ in the V−H stretching region may be compared with the symmetric and antisymmetric stretching bands for $VH_2$ at 1532.4 and 1508.3 $cm^{-1}$, respectively.[31] However, the binary vanadium hydrides were not observed in this study. The strong deuterium counterpart at 1106.5 $cm^{-1}$ (H/D isotopic ratio of 1.387) is near the symmetric and antisymmetric stretching frequencies for $VD_2$ at 1111.5 and 1079.5 $cm^{-1}$. On this basis, the single primary product of the V + $CH_4$ reaction is identified as the monohydrido C−H insertion product, $CH_3$−VH. The decrease on annealing to allow further reaction shows that the primary reaction is not spontaneous and that this primary product is a reactive species. Furthermore, methane activation by the $V^+$ ion was studied previously using ion beam techniques, and the $V^+$ + $CH_4$ reaction most likely proceeds via oxidative addition to the C−H bond to yield $CH_3$−$VH^+$.[32]

The absorptions at 541.6 and 510.1 $cm^{-1}$ in Figure 1 most likely originate from the C−V−H bending and C−V stretching modes. The former shifts to 464.7 $cm^{-1}$ (H/D isotopic ratio 1.165). In the $C_s$ structure with a bent C−V−H moiety for $CH_3$−VH, the two modes are heavily mixed. The observed frequencies are compared with the calculated values in Table 1. Clearly, the three absorptions are predicted to be the strongest in our observable region.

Our recent studies of metal atom reactions with methane or methyl halides show that Cr also forms only a mono-insertion product ($CH_3$−CrX), unlike the group 4 and group 6 transition metals, which form high-oxidation-state complexes along with the mono-insertion products. Computation results show that the Cr mono-insertion products are much more stable relative to the double and triple-bonded products.[13] In contrast, the single and double-bonded products ($CH_3$−MX and $CH_2$═MHX) for the group 4, and these plus the triple-bonded products (CH≡$MH_2$X) for group 6 transition metals have similar energies, and as a result, they are all formed in the reaction with $CH_3$X or subsequent photolysis.[4−15]

Vanadium is similar to its first-row neighbor Cr giving only the mono-insertion product ($CH_3$−VH), which is 34 kcal/mol more stable than $CH_2$═$VH_2$ in the doublet ground state. Unlike the singlet CH≡$VH_3^-$ anion, the doublet CH≡$VH_3$ neutral species converges to the structure $CH_2$═$VH_2$ instead. Clearly, vanadium is a very effective transition metal for preparation of the mono-insertion product of methane, due to the high reactivity and selectivity. The insertion reaction is promoted by irradiation that most effectively overlaps the strong 370 nm absorption of vanadium atoms in solid argon,[33] and the methylidene is too

**TABLE 8: Observed and Calculated Fundamental Frequencies of $CH_2{=}TaH_2$ Isotopomers**

(a) Configuration 1 in the $C_1$ Symmetry Ground $^2A$ Electronic State[a]

| approximate description | $CH_2{=}TaH_2$ freq obs | freq calc | int | $CD_2{=}TaD_2$ freq obs | freq calc | int | $^{13}CH_2{=}TaH_2$ freq obs | freq calc | int | CHD=TaHD freq obs | freq calc | int |
|---|---|---|---|---|---|---|---|---|---|---|---|---|
| C−H str | | 3189.0 | 1 | | 2360.4 | 3 | | 3178.1 | 1 | | 2338.4 | 5 |
| C−H str | | 2921.8 | 2 | | 2126.7 | 3 | | 2915.0 | 2 | | 2934.6 | 2 |
| Ta−H str | 1753.8 | 1799.0 | 193 | 1255.6 | 1275.1 | 105 | 1753.8 | 1799.0 | 193 | 1742.5 | 1794.1 | 264 |
| Ta−H str | 1731.9 | 1773.8 | 419 | 1243.6 | 1259.9 | 206 | 1731.9 | 1773.8 | 419 | 1249.8 | 1262.4 | 179 |
| $CH_2$ scis | | 1309.5 | 16 | | 1032.0 | 23 | | 1300.1 | 15 | | 1180.4 | 11 |
| C=Ta str | 825.6 | 818.4 | 62 | 740.0 | 692.5 | 34 | 803.4 | 807.3 | 58 | 780.0 | 761.5 | 51 |
| $TaH_2$ scis | | 734.1 | 2 | | 543.3 | 18 | | 724.0 | 3 | | 682.7 | 3 |
| $CH_2$ wag | 637.7 | 689.5 | 97 | 522.5 | 538.3 | 51 | | 683.6 | 94 | | 577.7 | 77 |
| $TaH_2$ rock | | 597.5 | 5 | | 455.5 | 3 | | 593.3 | 5 | | 480.3 | 5 |
| $CH_2$ twist | | 408.9 | 2 | | 290.4 | 1 | | 408.7 | 2 | | 359.6 | 2 |
| $CH_2$ rock | | 197.5 | 10 | | 142.4 | 5 | | 197.1 | 10 | | 165.9 | 5 |
| $TaH_2$ wag | | 123.5 | 81 | | 88.5 | 42 | | 123.5 | 81 | | 106.6 | 61 |

(b) Configuration 2 in the $C_s$ Symmetry Ground $^2A'$ Electronic State[b]

| approximate description | $CH_2{=}TaH_2$ freq obs | freq calc | int | $CD_2{=}TaD_2$ freq obs | freq calc | int | $^{13}CH_2{=}TaH_2$ freq obs | freq calc | int | CHD=TaHD freq obs | freq calc | int |
|---|---|---|---|---|---|---|---|---|---|---|---|---|
| A′ C−H str | | 3182.6 | 11 | | 2358.0 | 13 | | 3171.6 | 11 | | 2333.6 | 13 |
| A′ C−H str | | 2509.9 | 9 | | 1826.8 | 3 | | 2504.2 | 9 | | 2530.4 | 8 |
| A′ Ta−H str | 1753.8 | 1789.3 | 155 | 1255.6 | 1268.0 | 78 | 1753.8 | 1789.3 | 156 | 1742.5 | 1782.7 | 211 |
| A′ $CH_2$ scis | | 1317.8 | 27 | | 1021.4 | 19 | | 1310.4 | 27 | | 1221.1 | 17 |
| A′ C=Ta str | 825.6 | 847.2 | 58 | 740.0 | 742.8 | 38 | 803.4 | 820.0 | 56 | 780.0 | 792.2 | 47 |
| A′ $TaH_2$ scis | 637.7 | 678.3 | 26 | | 483.1 | 14 | | 678.0 | 26 | | 588.4 | 20 |
| A′ $TaH_2$ wag | | 560.2 | 37 | | 414.4 | 15 | | 558.5 | 37 | | 529.5 | 23 |
| A′ $CH_2$ rock | | 496.6 | 5 | | 366.0 | 7 | | 494.1 | 4 | | 417.4 | 10 |
| A″ Ta−H str | 1731.9 | 1776.4 | 272 | 1243.6 | 1262.4 | 140 | 1731.9 | 1776.4 | 272 | 1249.8 | 1265.6 | 112 |
| A″ $CH_2$ wag | 584.9 | 576.4 | 78 | | 450.6 | 37 | | 572.0 | 79 | | 473.2 | 41 |
| A″ $TaH_2$ twist | | 485.5 | 28 | | 350.4 | 22 | | 484.1 | 26 | | 368.9 | 27 |
| A″ $CH_2$ twist | | 206.1 | 2 | | 146.5 | 1 | | 206.1 | 2 | | 186.5 | 1 |

[a] B3LYP/6-311++G(3df,3pd)/SDD level. Frequencies and intensities are in $cm^{-1}$ and km/mol. Infrared intensities are calculated values. [b] BPW91/6-311++G(3df,3pd)/SDD level. Frequencies and intensities are in $cm^{-1}$ and km/mol. Infrared intensities are calculated values.

**TABLE 9: Observed and Calculated Fundamental Frequencies of $CH_3{-}TaH$ Isotopomers in the Ground $^4A''$ Electronic State[a]**

| approximate description | $CH_3{-}TaH$ freq obs | freq calc | int | $CD_3{-}Ta{-}D$ freq obs | freq calc | int | $^{13}CH_3{-}TaH$ freq obs | freq calc | int | $CHD_2{-}TaH$ freq obs | freq calc | int | $CH_2D{-}TaD$ freq obs | freq calc | int |
|---|---|---|---|---|---|---|---|---|---|---|---|---|---|---|---|
| A′ $CH_3$ str | | 3047.1 | 9 | | 2254.1 | 4 | | 3036.9 | 9 | | 2017.4 | 11 | | 3005.0 | 2 |
| A′ $CH_3$ str | | 2970.5 | 4 | | 2128.1 | 0 | | 2967.7 | 4 | | 2173.5 | 0 | | 2204.8 | 4 |
| A′ Ta−H str | 1726.2 | 1749.4 | 269 | 1236.8 | 1241.2 | 136 | 1726.0 | 1749.4 | 269 | 1724.6 | 1749.3 | 269 | *b* | 1241.1 | 137 |
| A′ $CH_3$ scis | | 1408.3 | 3 | | 1022.0 | 2 | | 1405.2 | 3 | | 1121.3 | 3 | | 1378.0 | 3 |
| A′ $CH_3$ deform | | 1169.7 | 8 | | 923.8 | 18 | | 1159.6 | 7 | | 963.1 | 12 | | 1089.4 | 9 |
| A′ CTaH bend | | 597.1 | 24 | | 462.3 | 30 | | 593.3 | 23 | | 557.3 | 10 | | 522.9 | 38 |
| A′ C−Ta str | | 485.5 | 35 | | 431.2 | 6 | | 485.5 | 35 | | 480.9 | 47 | | 431.9 | 5 |
| A′ $CH_3$ rock | | 337.6 | 12 | | 240.8 | 7 | | 337.2 | 11 | | 303.4 | 7 | | 254.1 | 9 |
| A″ $CH_3$ str | | 3051.4 | 4 | | 2254.3 | 1 | | 3040.9 | 4 | | 2254.4 | 1 | | 3051.1 | 3 |
| A″ $CH_3$ scis | | 1410.8 | 6 | | 1023.8 | 4 | | 1407.6 | 6 | | 1260.2 | 7 | | 1208.2 | 4 |
| A″ $CH_2$ twist | | 388.6 | 2 | | 288.4 | 1 | | 386.9 | 2 | | 295.3 | 0 | | 375.7 | 3 |
| A″ $CH_3$ distort | | 171.3 | 17 | | 122.3 | 9 | | 171.2 | 17 | | 153.6 | 22 | | 136.6 | 7 |

[a] B3LYP/6-311++G(3df,3pd)/SDD level. Frequencies and intensities are in $cm^{-1}$ and km/mol. Infrared intensities are calculated values. [b] Overlapped by a precursor absorption.

high in energy to form here.

$$V^* + CH_4 \rightarrow CH_3{-}VH \quad (1)$$

The structure of $CH_3{-}VH$ in the quartet ground state is shown in Figure 10. The molecule has $C_s$ symmetry, where the carbon, vanadium, and two hydrogen atoms lie in the molecular plane. The C−V bond length of 2.074 Å is compared with that of 2.072 Å of $V\{\eta^2\text{-}C(Mes){=}NBu^t\}_3$ (Mes = 2,4,6-$Me_3C_6H_2$).[34] The C−V and V−H bonds are highly polarized with Mulliken atomic charges for C, V, $H_1$, $H_2$, and $H_4$ of −0.34, 0.62, 0.01, −0.01, and −0.27, respectively, and the dipole moment is 2.65 D. The unobserved higher-energy $CH_2{=}VH_2$ structure is also given for comparison.

**Nb + $CH_4$.** The spectra observed for Nb and Ta reveal a one to one correspondence among the observed four absorption band groups. Each set of absorptions is due to a different product based on their variations upon photolysis, annealing, and addition of a trace of $CCl_4$ or $CBr_4$. The consistent agreement between the Nb and Ta spectra helps to substantiate the assignments.

The two absorptions marked **m** at 1680.7 and 1652.5 $cm^{-1}$ in the Nb−H stretching region (Figure 2) show a constant 1:2

**TABLE 10: Observed and Calculated Fundamental Frequencies of $CH{\equiv}TaH_3^-$ Isotopomers in the Ground $^1A_1$ Electronic State[a]**

| approximate description | $CH{\equiv}TaH_3^-$ | | | $CD{\equiv}TaD_3^-$ | | | $^{13}CH{\equiv}TaH_3^-$ | | | $CH{\equiv}TaHD_2^-$ | | | $CD{\equiv}TaDH_2^-$ | | |
|---|---|---|---|---|---|---|---|---|---|---|---|---|---|---|---|
| | freq | | | freq | | | freq | | | freq | | | freq | | |
| | obs | calc[b] | int | obs | calc[b] | int | obs | calc[b] | int | obs | calc[b] | int | obs | calc[b] | int |
| $A_1$ C−H str | | 3141.7 | 12 | | 2330.0 | 0 | | 3130.6 | 13 | | 3141.7 | 12 | | 2330.1 | 0 |
| $A_1TaH_3$ str | *b* | 1646.2 | 401 | 1160.9 | 1166.1 | 182 | *b* | 1646.1 | 403 | 1585.2 | 1607.9 | 566 | 1604.6 | 1627.7 | 485 |
| $A_1$ C≡Ta str | 917.6 | 945.8 | 182 | 862.8 | 899.4 | 152 | 889.0 | 915.6 | 175 | 916.1 | 941.5 | 173 | | 903.7 | 166 |
| $A_1$ $TaH_3$ deform | | 624.5 | 94 | | 447.0 | 51 | | 623.6 | 91 | | 570.0 | 79 | | 567.2 | 80 |
| E $TaH_3$ str | 1567.8 | 1588.7 | 683 × 2 | 1126.6 | 1130.3 | 351 × 2 | 1567.7 | 1588.6 | 682 × 2 | 1150.2 | 1153.9 | 247 | 1566.0 | 1587.7 | 667 |
| | | | | | | | | | | 1128.6 | 1132.0 | 373 | 1139.4 | 1143.1 | 320 |
| E $TaH_3$ scis | | 632.1 | 157 × 2 | | 448.3 | 129 × 2 | | 632.1 | 157 × 2 | | 579.6 | 183 | | 627.3 | 106 |
| | | | | | | | | | | | 573.6 | 116 | | 559.3 | 62 |
| E TaCH bend | 574.6 | 571.8 | 72 × 2 | | 447.1 | 1 × 2 | 569.7 | 567.2 | 69 × 2 | | 544.3 | 10 | | 460.6 | 94 |
| | | | | | | | | | | | 447.3 | 45 | | 447.9 | 60 |
| E $TaH_3$ rock | | 450.4 | 0 × 2 | | 325.2 | 1 × 2 | | 449.6 | 0 × 2 | | 359.7 | 6 | | 394.9 | 7 |
| | | | | | | | | | | | 349.8 | 0 | | 353.9 | 10 |

[a] B3LYP/6-311++G(3df,3pd)/SDD level. Frequencies and intensities are in $cm^{-1}$ and km/mol. Infrared intensities are calculated values. [b] Probably overlapped by the water absorption at 1623.6 $cm^{-1}$.

**TABLE 11: Observed and Calculated Frequencies of Strong Fundamentals of $(CH_3)_2TaH_2$ Isotopomers in the Ground $^2A_2$ Electronic State[a]**

| approximate description | $(CH_3)_2TaH_2$ | | | $(CD_3)_2TaD_2$ | | | $(^{13}CH_3)_2TaH_2$ | | | $C_2H_3D_3TaHD$ | | |
|---|---|---|---|---|---|---|---|---|---|---|---|---|
| | freq | | | freq. | | | freq. | | | freq. | | |
| | obs | calc | int | obs | calc | int | obs | calc | int | obs | calc | int |
| $\nu_1$ $A_1$ $CH_3$ str | 2890.2 | 3035.3 | 24 | | 2235.4 | 10 | | 3026.5 | 24 | | 3047.2 | 13 |
| $\nu_3$ $A_1$ $TaH_2$ str | 1787.8 | 1817.7 | 256 | 1275.4 | 1288.0 | 130 | 1787.8 | 1817.7 | 256 | 1771.6 | 1804.3 | 295 |
| $\nu_{16}$ $B_1$ $TaH_2$ str | 1761.4 | 1791.1 | 341 | 1260.3 | 1272.8 | 174 | 1761.4 | 1791.1 | 340 | 1270.4 | 1280.8 | 158 |
| $\nu_6$ $A_1$ $TaH_2$ scis | | 681.6 | 80 | | 514.6 | 46 | | 680.8 | 78 | | 605.5 | 58 |
| $\nu_{26}$ $B_2$ $TaH_2$ wag | | 508.0 | 158 | | 382.4 | 42 | | 501.2 | 164 | | 473.1 | 80 |

[a] B3LYP/6-311++G(3df,3pd)/SDD level. Frequencies and intensities are in $cm^{-1}$ and km/mol. Infrared intensities are calculated values.

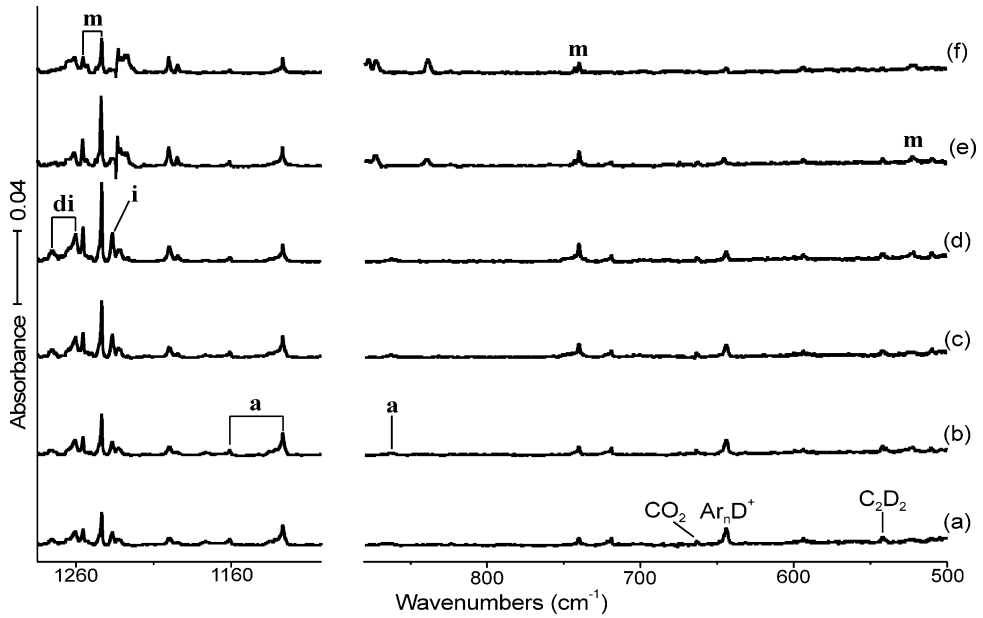


**Figure 7.** IR spectra in the regions of 1285−1100 and 880−500 $cm^{-1}$ for laser-ablated Ta atoms co-deposited with $CD_4$ in excess argon at 8 K. (a) Ta + 2% $CD_4$ in Ar co-deposited for 1 h. (b) After broad-band photolysis with a filter ($\lambda$ > 420 nm) for 20 min. (c) After broad-band photolysis with a filter (240 < $\lambda$ < 380 nm) for 20 min. (d) After broad-band photolysis with a filter ($\lambda$ > 220 nm) for 20 min. (e) After annealing to 26 K. (f) After annealing to 32 K. **m**, **i**, **a**, and **di** stand for the product absorption groups.

intensity ratio. The $^{13}C$ substitution leads to negligible frequency shift, whereas deuteration results in frequency shifts of −474.7 and −463.0 $cm^{-1}$ (H/D isotopic ratios of 1.394 and 1.389), suggesting that they arise from the symmetric and antisymmetric stretching modes of the Nb methylidene (dihydrido) complex ($CH_2{=}NbH_2$). These modes are slightly higher than those for $NbH_2$ (1610.4 and 1569.1 $cm^{-1}$).[30] The absorption observed at 805.4 $cm^{-1}$ shows $^{13}C$ and D frequency shifts of −20.9 and −68.6 $cm^{-1}$ ($^{12}C/^{13}C$ and H/D isotopic ratios of 1.027 and 1.093). Due to the frequency and relatively large $^{13}C$ shift, the band is due to the mostly C=Nb stretching mode. The absorptions at 547.1 and 480.1 $cm^{-1}$ in the further lower frequency region exhibit very small (−0.5 $cm^{-1}$) and negligible $^{13}C$ frequency shifts (D counterparts are not observed due to the low frequencies), respectively, and are assigned to the $CH_2$ wagging and $NbH_2$ twisting modes. The observed fre-

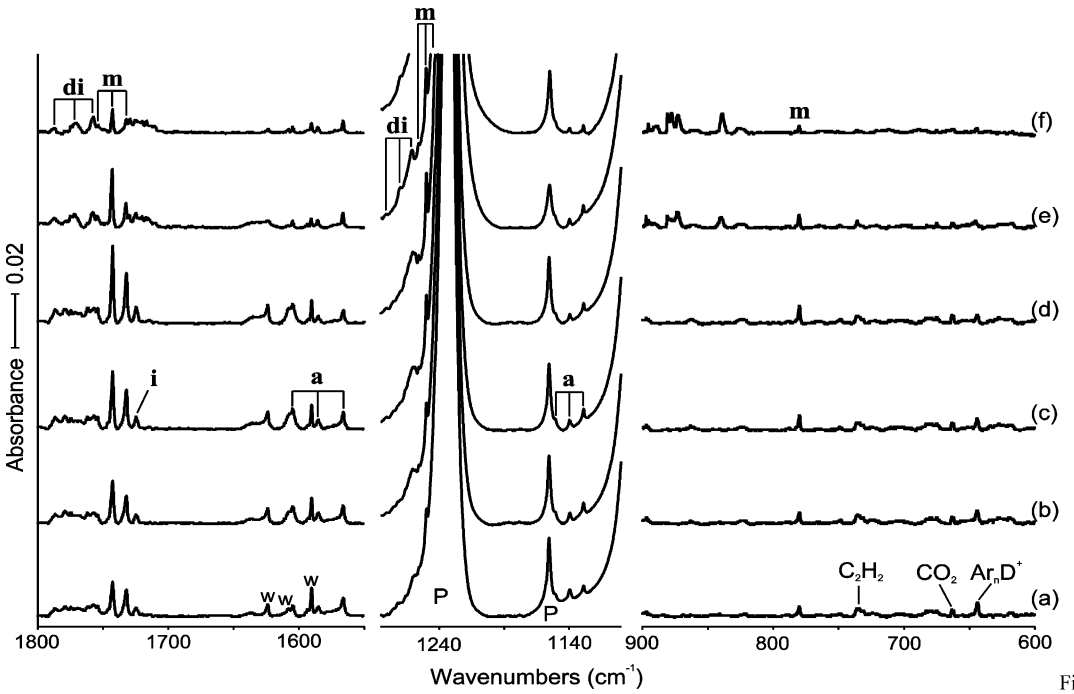


Fig 8

**Figure 8.** IR spectra in the regions of 1800−1550, 1285−1100, and 900−600 $cm^{-1}$ for laser-ablated Ta atoms co-deposited with $CH_2D_2$ in excess argon at 8 K. (a) Ta + 2% $CH_2D_2$ in Ar co-deposited for 1 h. (b) After broad-band photolysis with a filter ($\lambda$ > 420 nm) for 20 min. (c) After broad-band photolysis with a filter (240 < $\lambda$ < 380 nm) for 20 min. (d) After broad-band photolysis with a filter ($\lambda$ > 220 nm) for 20 min. (e) After annealing to 26 K. (f) After annealing to 32 K. **m**, **i**, **a**, and **di** stand for the product absorption groups. "P" and "w" denote the precursor and water residue absorptions, respectively.

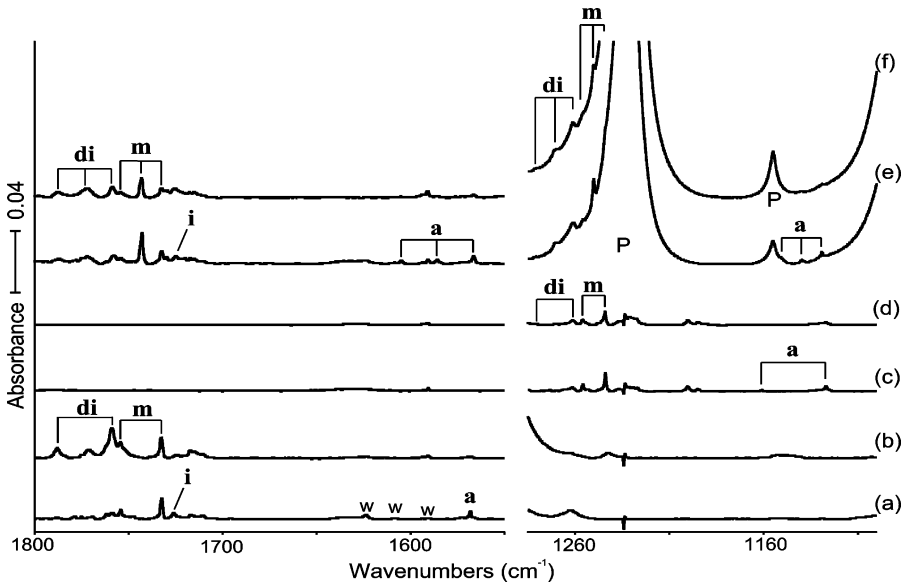


**Figure 9.** IR spectra in the regions of 1800−1550 and 1285−1100 $cm^{-1}$ for laser-ablated Ta atoms after annealing to 26 K following co-deposition of Ta atoms with $CH_4$ isotopomers in excess argon at 8 K for 1 h: (a) 1% $CH_4$; (b) 5% $CH_4$; (c) 2% $CD_4$; (d) 5% $CD_4$; (e) 2% $CH_2D_2$; (f) 5% $CH_2D_2$. **m**, **i**, **a**, and **di** stand for the product absorption groups. "P" and "w" denotes the precursor absorption.

quencies are compared with the calculated frequencies in Table 3, where the BPW91 vibrational frequencies are generally in better agreements with the observed values than the B3LYP values.

Methylidene complexes of group 4 and 6 transition metals ($CH_2$═MHX) have been prepared by α-hydrogen migration in the mono-insertion complexes ($CH_3$−MX) during co-deposition of the metal atom and $CH_3X$ or photolysis afterward, and several of these processes are photoreversible.[4−15] However, the Nb + $CH_4$ system is apparently not photoreversible, but the increases in absorption intensity of the **m** absorptions on photolysis are remarkable, particularly upon visible and full-arc irradiation. Apparently, our "420 nm" long-wavelength pass filter reaches the red tail of the 400 nm Nb atom absorption in solid argon and initiates reaction, which continues with strong absorption at 344 nm in the near-ultraviolet.[35]

$$Nb^* + CH_4 \rightarrow CH_3{-}NbH \rightarrow CH_2{=}NbH_2 \qquad (2)$$

The $CH_2D_2$ spectra in Figure 4 provide diagnostic information about the structure of $CH_2$═$NbH_2$: Two strong absorptions appear at 1666.4 and 1198.4 $cm^{-1}$ at the middle of the metal−hydrogen stretching absorption pairs of $CD_2$═$NbH_2$ and $CH_2$═$NbD_2$, respectively, which occur almost unshifted from pure

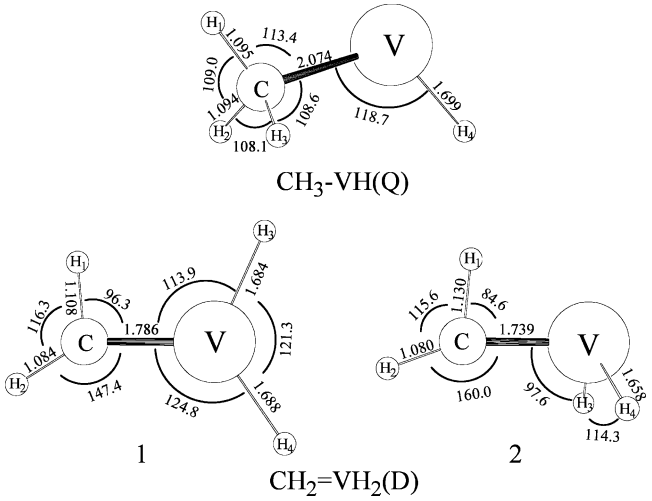


**Figure 10.** Optimized structures of $CH_3-VH(Q)$ and $CH_2=VH_2(D)$ configurations at the level of B3LYP/6-311++G(3df,3pd). All electron basis is used for V. Q and D denote quartet and doublet electronic states. The bond lengths and angles are in Å and degrees.

(all H or all D) isotopic values. This result strongly suggests that the two metal−hydrogen bonds are identical. Deuteration of one of the hydrogen atoms breaks the coupling between the two hydrogen stretching motions of the $NbH_2$ group, and if the metal−hydrogen bonds are identical, the hydrogen stretching absorption (free from the coupling) should appear at the median of the symmetric and antisymmetric hydrogen stretching pair.

It must be remembered that the methylidene dihydride complexes formed in previous studies from methane and groups 4 and 6 transition metals show spectroscopic evidence for two different metal−hydrogen bonds, due to the agostic interaction.[8−13] The agostic structure with distorted $CH_2$ subgroup and two different metal−hydrogen bonds are reproduced by electronic structure computations, and the predicted vibrational characteristics are in good agreement with the observed values.

Calculations at the B3LYP, BPW91, and MP2 levels with medium or large basis all give a stable $C_1$ structure doublet ground state (configuration 1 in Figure 11), where the $CH_2$ group is considerably distorted (the agostic angle is 99.7°, and $r$(Nb···H) is 2.350 Å with B3LYP/6-311++G(3df,3pd)), showing the agostic interaction. Due to the distorted $CH_2$ subgroup, the two metal−hydrogen bonds are inevitably different from each other. This $C_1$ structure for $CH_2=NbH_2$ is consistent with those of the methylidene hydride complexes of groups 4 and 6 transition metals, and the agostic angle of 99.7° is compared to those of 92.9 and 113.0° for $CH_2=ZrH_2$ and $CH_2=MoH_2$, respectively.

However, further investigation for the structure of $CH_2=NbH_2$ leads to another stable configuration (configuration 2) with $C_s$ symmetry, as shown in Figure 11, which is only 0.9, 0.2, and 2.9 kcal/mol higher in energy at the levels of B3LYP, BPW91, and MP2/6-311++G(3df,3pd), respectively, and probably within the accuracy of the calculations even if basis set superposition error were taken into account. Furthermore, matrix interaction could also reverse such a small energy difference. Hence, configurations 1 and 2 for $CH_2=NbH_2$ are essentially isoergic under our experimental and theoretical conditions. The predicted frequencies for configurations 1 and 2 are compared with observed values in Table 3a,b. Note that the two metal−hydrogen bonds are identical in configuration 2, and interestingly enough, the agostic interaction appears to be even stronger (the agostic angle is 83.1°, and $r$(Nb···H) is 2.061 Å). The agostic distortion is a structural rearrangement to stabilize the carbon−

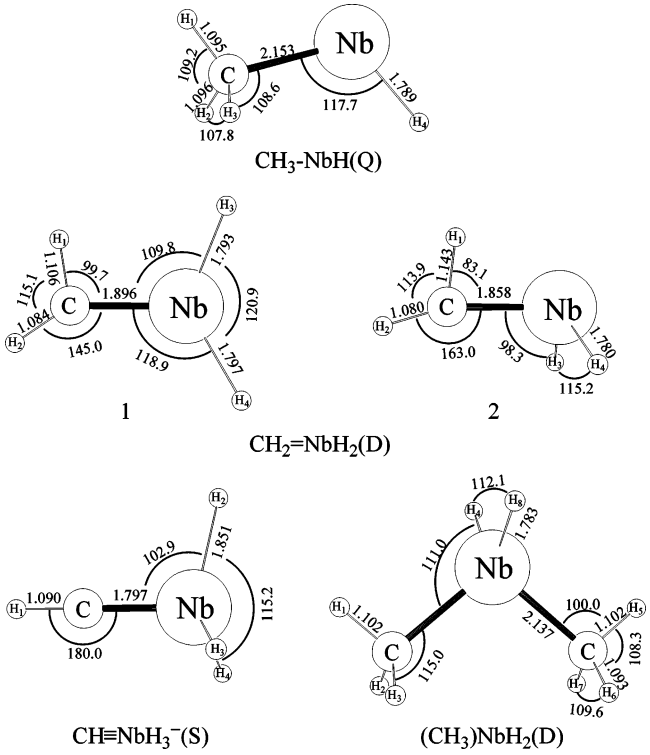


**Figure 11.** Optimized structures of $CH_3-NbH(Q)$, $CH_2=NbH_2(D)$, $CH\equiv NbH_3^-(S)$, and $(CH_3)_2NbH_2(D)$ at the level of B3LYP/6-311++G(3df,3pd)/SDD. The bond lengths and angles are in Å and degrees. Q, D, and S indicate quartet, doublet and singlet state multiplicity.

metal bond and closely related to the C=M bond length, and the shorter carbon−metal bond is normally accompanied by the stronger agostic interaction.[9−13] The carbon−metal bond lengths of 1.896 and 1.858 Å in configurations 1 and 2 are compared to 1.94−2.00 Å values for large alkylidene complexes.[1]

The new $C_s$ structure predicted for the Nb methylidene hydride is quite unique. The previously studied methylidene hydride complexes of groups 4 and 6 transition metals converge to $C_1$ structures with two slightly different metal−hydrogen bonds. Calculations show that the V and Ta methylidene hydride complexes also have the stable $C_s$ configurations almost equal in energy with the $C_1$ structure. The $C_s$ structure is apparently more favorable for the methylidene hydride complexes in the doublet ground state. The spectrum of the methylidene hydride complex using $CH_2D_2$ suggests two identical Nb−H bonds and requires configuration 2, although its energy is slightly higher than the global energy minimum (configuration 1). In an effort to further examine the molecular structure of $CH_2=NbH_2$, calculations with CCSD/6-311++G(2d,p)/SDD were performed, and the results also show that configuration 1 is the global minimum, whereas configuration 2 is 3.2 kcal/mol higher in energy.

It should also be noted here that the T1 diagnostic values in the CCSD calculations for doublet $CH_2=NbH_2$ are in the range 0.05−0.07, which are higher than the 0.02 value where a multiconfiguration calculation may be required.[36] This indicates that multiconfiguration calculations are necessary to search for the structure of $CH_2=NbH_2$, and that there is the possibility that neither configuration 1 nor configuration 2 in Figure 11 may represent the exact molecular structure of the methylidene hydride complex. The niobium methylidene hydride complex poses a challenge to electronic structure theory, which is beyond the scope of this work.

The single absorption marked **i** at 1611.4 $cm^{-1}$ is observed on the red side of the **m** absorptions in Figure 2. The absorption does not show dramatic increase in intensity in the process of photolysis, unlike the **m** absorptions. The $^{13}C$ substitution leads to a negligible shift, but deuteration gives a large shift of −452.3 $cm^{-1}$ (H/D isotopic ratio of 1.390), suggesting that the band originates from the Nb−H stretching mode of a monohydrido insertion product. The low-frequency absorptions are not observed in this study due to low intensities. In the previous studies on methane activation by group 4 and 6 transition metals,[8−13] the metal−hydrogen stretching band of $CH_3-MH$ appears on the red side of the hydrogen stretching absorption pair of the methylene dihydride complex.

In the reaction of transition-metal atoms and methane, the monohydrido insertion product is formed first.[9,12,37−39] The appearance of $CH_3-VH$ in the reaction of V with $CH_4$ described above is another example. High-oxidation-state transition-metal complexes ($CH_2{=}MH_2$ and $CH{\equiv}MH_3$) are formed most likely from the monohydrido complex via α-hydrogen migration.[8−13] The reaction to give $CH_3-MH$ requires activation energy, laser ablation provides excited transition-metal atoms, and the excited intermediate thus formed can be relaxed by the matrix or undergo α-hydrogen transfer. The absorptions marked **i** in Figures 2−6 are assigned to $CH_3-NbH$ in the quartet ground state.

The predicted frequencies for $CH_3-NbH$ are listed in Table 4. The observed hydrogen stretching band is in fact the strongest one among the IR absorptions; the second strongest band is expected a sixth as strong as the Nb−H stretching band. The predicted structure of $CH_3-NbH$ is shown in Figure 11, which the carbon, niobium, and two hydrogen atoms are in the molecular plane, similar to the structure of $CH_3-VH$ in Figure 10. The C−Nb bond length of 2.153 Å is substantially longer than that of $CH_2{=}NbH_2$ and compared to that of 2.228 Å measured for $Tp^{Me_2}NbCl(i\text{-}Pr)(PhC{\equiv}CMe)$ [$Tp^{Me_2}$ = hydrotris-(3,5-dimethylpyrazolyl)borate].[40] The geometrical and other physical parameters of $CH_3-NbH$ are listed in Table 12.

The absorptions marked **a** at 1542.5 and 1489.5 $cm^{-1}$ are observed on the red side of the Nb−H stretching region, as shown in Figure 2. The $^{13}C$ substitution gives negligible shifts, but deuteration leads to frequency shifts of −438.8 and −413.4 $cm^{-1}$ (H/D isotopic ratios of 1.398 and 1.384), respectively, indicating that they are Nb−H stretching absorptions. However, the frequencies are exceptionally low in comparison with other Nb−H stretching frequencies of neutral niobium hydrides (e.g., 1708.0, 1705.2, 1688.4, and 1683.9 $cm^{-1}$ for $NbH_4$, 1610.4 and 1569.1 $cm^{-1}$ for $NbH_2$, and 1555.9 $cm^{-1}$ for NbH) and the latter two bands are detected here.[30] Moreover, the absorptions completely disappear on addition of a trace of $CCl_4$ (Figure 2a). Earlier studies show that the concentration of an anionic product dramatically decreases upon addition of $CCl_4$ by removing electrons produced in the laser-ablation process.[26] Depletion of the absorptions by addition of $CCl_4$, along with the exceptionally low hydrogen stretching frequencies, indicates that the absorptions at 1542.5 and 1489.5 $cm^{-1}$ originate from an anionic product with at least two hydrogen atoms bonded to the Nb atom.

The energies of the plausible products relative to that of the niobium atom ($^6D_{1/2}$) and $CH_4$ are shown in Figure 12. It is notable that, $CH_3-NbH$ and $CH_2{=}NbH_2$ in the quartet and doublet ground states, respectively, are energetically close to each other and the most stable among the primary neutral products. On the other hand, among the anionic products, $CH{\equiv}NbH_3^-$ in the singlet ground state is clearly the most stable species. In recent matrix studies on reaction of group 6 transition metals (Mo and W) with $CH_4$,[12,13] the simplest possible methylidyne trihydride complex, $CH{\equiv}MH_3$, is formed along with $CH_3-MH$ and $CH_2{=}MH_2$. The three C−H insertion products are interconvertible via α-hydrogen migration upon visible and near UV irradiation. With addition of an electron to the Nb atom, it becomes isoelectronic with the Mo atom, having six electrons in the valence shell ($5s^14d^5$), and electron capture by $CH_2{=}NbH_2$ thus results in rearrangement to the more stable methylidyne anion.

$$CH_2{=}NbH_2 + e^- \rightarrow [CH_2{=}NbH_2]^- \rightarrow CH{\equiv}NbH_3^- \quad (3)$$

The energies displayed in Figure 12 also suggest that loss of an electron from $CH{\equiv}NbH_3^-$ would lead to formation of $CH_3-NbH$ or $CH_2{=}NbH_2$. The $CH{\equiv}NbH_3$ neutral doublet ground state is higher than the reactants (Nb($^6D$) + $CH_4$)), and therefore, the neutral niobium methylidyne hydride complex most likely transforms to the more stable mono- or dihydrido insertion product. It is in fact shown in Figures 2−5 that decreases of the **a** absorptions upon full-arc irradiation are accompanied by increases in the absorptions of the methylidene dihydride complex.

The $CH{\equiv}NbH_3^-$ anion is calculated to have the $C_{3v}$ structure shown in Figure 11. Despite the negative charge, the C−Nb bond length of 1.797 Å is much shorter than those of $CH_3-NbH$ and $CH_2{=}NbH_2$ but longer than the C−Mo bond length of 1.714 Å for neutral $CH{\equiv}MoH_3$. The predicted frequencies for the isotopomers are compared with the observed values, as in Table 5, which are in good agreement. The observed/calculated ratios for the hydrogen stretching absorptions of $CH{\equiv}NbH_3^-$, $^{13}CH{\equiv}NbH_3^-$, and $CD{\equiv}NbD_3^-$ are 0.968, 0.967, 0.968, 0.967, 0.978, and 0.977, respectively. The vibrational characteristics of other plausible products are also examined,

**TABLE 12: Geometrical Parameters and Physical Constants of $CH_3-NbH$, $CH_2{=}NbH_2$, $CH{\equiv}NbH_3^-$, and $(CH_3)_2NbH_2$[a]**

| | | $CH_2{=}NbH_2$ | | | |
|---|---|---|---|---|---|
| parameters | $CH_3-NbH$ | config. 1 | config. 1 | $CH{\equiv}NbH_3^-$ | $(CH_3)_2NbH_2$ |
| $r$(C−Nb) | 2.153 | 1.896 | 1.858 | 1.797 | 2.137 |
| $r$(C−$H_1$) | 1.095 | 1.106 | 1.143 | 1.090 | 1.102 |
| $r$(C−$H_2$) | 1.096 | 1.084 | 1.080 | | 1.093 |
| $r$(Nb−$H_3$) | | 1.793 | 1.780 | 1.851 | |
| $r$(Nb−$H_4$) | 1.787 | 1.797 | 1.780 | 1.851 | 1.783 |
| $r$(Nb···$H_1$) | 2.774 | 2.350 | 2.060 | 2.887 | 2.569 |
| ∠$H_1CH_2$ | 109.2 | 115.1 | 113.9 | | 108.3 |
| ∠$H_2CH_3$ | 107.8 | | | | 109.6 |
| ∠$CNbH_3$ | | 109.8 | 98.3 | 102.9 | |
| ∠$CNbH_4$ | 117.7 | 118.9 | 98.3 | 102.9 | 111.0 |
| ∠$H_3NbH_4$ | | 120.9 | 115.2 | 115.2 | |
| ∠$H_1CNb$ | 113.2 | 99.7 | 83.1 | 180.0 | 100.0 |
| ∠$H_2CNb$ | 108.6 | 145.0 | 163.0 | | 115.0 |
| Φ($H_1CNbH_3$) | 121.5 | 174.0 | 121.4 | | 115.7 |
| Φ($H_1CNbH_4$) | 180.0 | 167.5 | −121.4 | | 62.7 |
| mol symm | $C_s$ | $C_1$ | $C_s$ | $C_{3v}$ | $C_{2v}$ |
| $q$(C)[b] | −0.92 | −0.79 | −0.66 | −0.97 | −0.85 |
| $q$($H_1$)[b] | 0.04 | 0.02 | −0.01 | 0.01 | 0.10 |
| $q$($H_2$)[b] | 0.08 | 0.00 | 0.02 | −0.58 | 0.05 |
| $q$($H_3$)[b] | 0.08 | −0.41 | −0.37 | −0.58 | 0.05 |
| $q$($H_4$)[b] | −0.41 | −0.44 | −0.37 | −0.58 | −0.42 |
| $q$(Nb)[b] | 1.14 | 1.63 | 1.40 | 1.68 | 2.15 |
| $\mu$[c] | 1.82 | 1.25 | 2.80 | 1.73 | 0.93 |
| state[d] | $^4A''$ | $^2A$ | $^2A'$ | $^1A_1$ | $^2A_2$ |
| $\Delta E$[e] | 17.6 | 19.7 | 18.8 | 60.6 (40.7[f]) | 47.9 |

[a] Bond lengths and angles are in Å and degree. Calculated at the level B3LYP/6-311++G(3df,3pd)/SDD. [b] Mulliken atomic charge. [c] Molecular dipole moment in D. [d] Electronic state. [e] Binding energies in kcal/mol relative to $CH_3F$ and Nb ($^6D$). [f] Binding energy in kcal/mol relative to $CH_3F$ and $^5Nb^-$ ($^5D$).

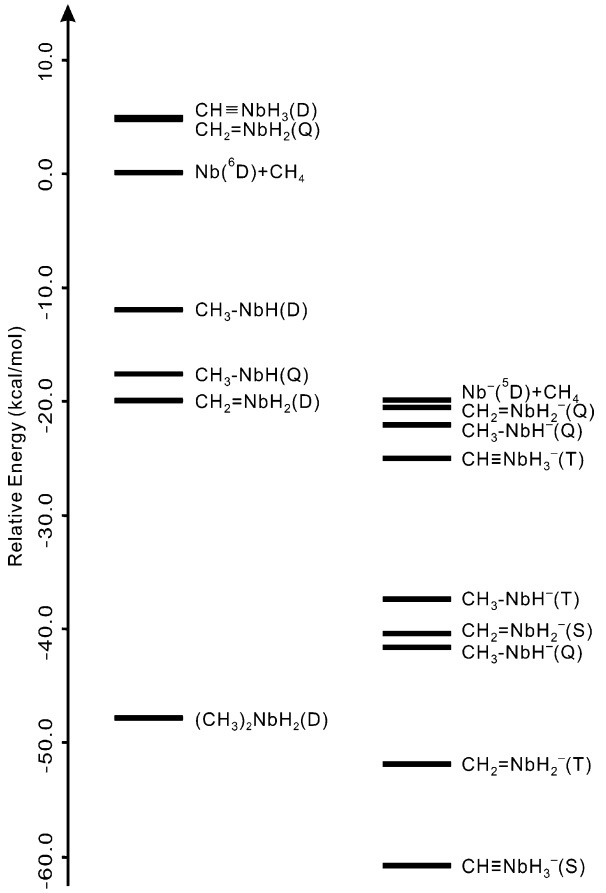


**Figure 12.** Energies of neutral and anionic products relative to Nb($^6$D) + $CH_4$. Note that $CH_3-NbH(Q)$ and $CH_2=NbH_2(D)$ are the most stable ones among the plausible neutral primary products. Formation of the high-order product, $(CH_3)_2NbH_2(D)$, brings further stabilization. Also note that $CH\equiv NbH_3^-(S)$ is the most stable among the plausible anionic products. S, D, and Q denote singlet, doublet, and quartet states.

but they do not match as well as those of $CH\equiv NbH_3^-$. Unfortunately, the low-frequency **a** absorptions are not observed, probably due to the low intensity. However, the **a** absorptions in the Ta spectra showing parallel characteristics are stronger, and the low-frequency components match well with the predicted values. On the basis of the experimental and computational results, the **a** absorptions are assigned to the anionic methylidyne complex, $CH\equiv NbH_3^-$. This observation is significant because the known carbynes are mostly group 6 transition-metal complexes, and attempts to synthesize anionic group 5 carbyne anion complexes have not been successful.[1] The methylidyne hydride complex, $CH\equiv NbH_3^-$, is the first group 5 transition-metal trihydride carbyne anion complex, and it may be compared with the $CH\equiv NbH_2F^-$ product from $CH_3F$ reactions with laser-ablated Nb.[18]

The absorptions marked **di** at 1717.5 and 1686.3 $cm^{-1}$ are not clearly discernible in the original spectrum after deposition but become stronger in the process of photolysis and early stage of annealing. Although $^{13}C$ substitution gives negligible shifts, deuteration causes large 486.0 and 473.3 $cm^{-1}$ red shifts (H/D isotopic ratios of 1.395 and 1.390). More importantly, their relative intensities to those of the other sets of absorptions increase markedly at high concentration of the precursor, and their metal−hydrogen stretching frequencies are higher than those of $CH_3-NbH$ and $CH_2=NbH_2$, probably due to the higher oxidation state of the metal atom. The observed spectroscopic characteristics suggest that the **di** absorptions arise form a higher-order product.

Earlier studies show that group 4 transition metals form dimethyl complexes ($(CH_3)_2MX_2$) in reaction with methane as well as methyl halides,[4,6−11] whereas group 6 transition metals evidently do not form the high-order complex.[12−15] The present results suggest that Nb, a group 5 transition metal, also forms a dimethyl dihydride complex ($(CH_3)_2NbH_2$) in reaction with methane and more in the following process of photolysis and annealing. But the bands are much weaker relative to those in the spectra of group 4 transition metals, indicating that the **di** complex is formed much less with the group 5 transition metal.

The observed metal−hydrogen stretching frequencies of the **di** absorptions are compared with those predicted frequencies for $(CH_3)NbH_2$ in Table 6. Evidently, the observed hydrogen stretching bands are the first and second strongest ones, and the other absorptions are much weaker. $(CH_3)NbH_2$ is computed to have a $C_{2v}$ structure as shown in Figure 11 and is in fact the most stable neutral product examined in this study (Figure 12), leading to increase of the product in the process of photolysis and annealing and particularly at high concentration of the precursor. The observation of two intermediate mixed isotopic bands with $CH_2D_2$ suggests that the two metal−hydrogen bonds may, however, be inequivalent in this doublet ground-state molecule.

The binding energy of $(CH_3)_2NbH_2$ is 30 and 28 kcal/mol larger than those of $CH_3-NbH$ and $CH_2=NbH_2$, respectively, as shown in Table 12. It is not clear at this point whether $(CH_3)_2NbH_2$ is formed in reaction of $CH_3-NbH$ or $CH_2=NbH_2$ with methane located nearby in the matrix. Alkylidene complexes are well-known C−H activation agents of alkane, and therefore, C−H activation of $CH_4$ by $CH_2=NbH_2$ should lead to $(CH_3)_2NbH_2$. Activation reaction of an alkane by an alkylidene complex is similar to an addition reaction to a double bond.

$$CH_2=NbH_2 + H-CH_3 \rightarrow (CH_3)_2NbH_2 \qquad \Delta E = -28 \text{ kcal/mol} \quad (4)$$

On the other hand, the $CH_3-NbH$ in the quartet state is also expected reactive enough with $CH_4$ for C−H insertion and to proceed to $(CH_3)_2NbH_2$.

$$CH_3-NbH(Q) + CH_4 \rightarrow (CH_3)_2NbH_2 \qquad \Delta E = -30 \text{ kcal/mol} \quad (5)$$

**Ta + $CH_4$.** Parallel to the case of Nb described above, four sets of product absorptions are observed in the spectra from reaction of Ta with $CH_4$, as shown in Figures 6−9, whereas the frequencies are in general a little higher due to the effect of relativity in the third-row transition metal series.[41] The strong **m** absorption pair at 1753.8 and 1731.9 $cm^{-1}$ increases on irradiation. The large increase in UV region arises from the strong electronic absorption of Ta at 260−270 nm.[42] The absorption pair shows essentially no shifts on $^{13}C$ substitution but gives shifts of −498.2 and −488.3 $cm^{-1}$ on deuteration (H/D isotopic ratios of 1.397 and 1.393), respectively, indicating that they are Ta−H stretching bands. The above m bands are very near 1759 and 1733 $cm^{-1}$ absorptions observed for $TaH_2$ in the Ta + $H_2$ reaction.[30b]

The band at 825.6 $cm^{-1}$ shifts 22.2 and 85.6 $cm^{-1}$ on $^{13}C$ and D substitutions ($^{12}C/^{13}C$ and H/D isotopic ratios of 1.028 and 1.116), respectively. The large $^{13}C$ shift indicates that the band arises from a vibrational mode involving considerable displacement of the carbon atom, and the relatively high frequency suggests a double bond between carbon and tantalum atoms. It is, therefore, assigned to the C=Ta stretching mode. The weak absorptions at 637.7 and 584.9 $cm^{-1}$ are due to the

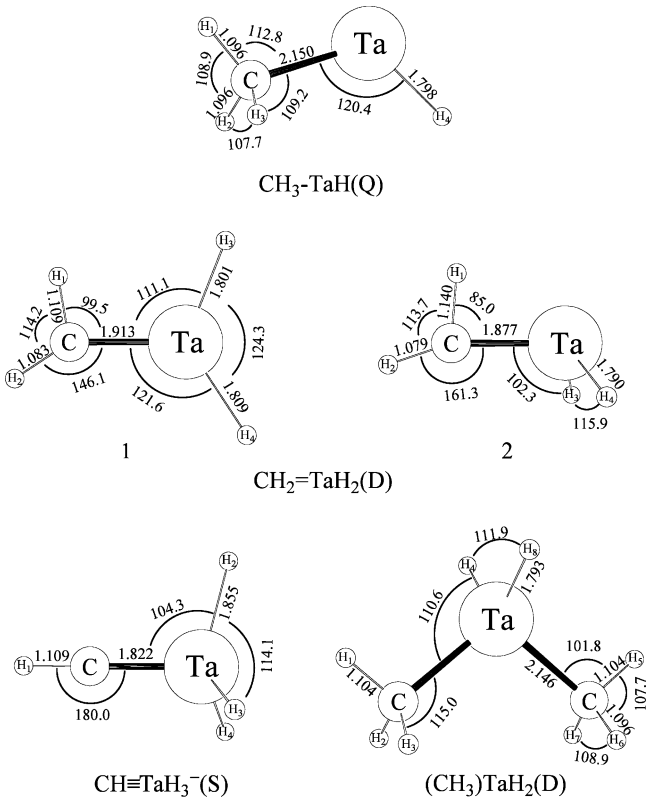


**Figure 13.** Optimized structures of $CH_3-TaH$(Q), $CH_2=TaH_2$(D), $CH\equiv TaH_3^-$(S), and $(CH_3)_2TaH_2$(D) at the level of B3LYP/6-311++G(3df,3pd)/SDD. The bond lengths and angles are in Å and degrees. Q, D, and S indicate quartet, doublet and singlet state multiplicity.

mostly $TaH_2$ scissoring and $CH_2$ wagging modes of the reaction product. The **m** absorptions are assigned to the Ta methylidene hydride complex, $CH_2=TaH_2$, consistent with the case of $CH_2=NbH_2$.

The strong sharp Ta−H and Ta−D stretching absorptions at 1742.6 and 1249.8 $cm^{-1}$ are observed in the $CH_2D_2$ spectra (Figure 8) and are near the median of the metal−hydrogen stretching absorption pairs of $CD_2=TaH_2$ and $CH_2=TaD_2$, respectively. In line with the Nb case, this indicates that the two metal−hydrogen bonds are identical, and calculations show that the $C_1$ structure with the distorted $CH_2$ group (configuration 1) in Figure 13 is the most stable. However, there is another stable structure with $C_s$ symmetry (configuration 2) 2.0 kcal/mol higher in energy, which contains two identical metal−hydrogen bonds. The geometrical and other physical parameters of $CH_3-TaH$ are listed in Table 13.

CCSD calculations were also carried out to examine the structure of the methylidene hydride complex, and similar to the case of $CH_2=NbH_2$, configuration 1 is 4.2 kcal/mol lower in energy than configuration 2. The T1 diagnostic values in CCSD calculations for $CH_2=TaH_2$ are near 0.060, which reaffirm that multiconfiguration calculations are necessary for investigation of the structures of the methylidene hydride complexes of group 5 transition metals. Although it is not calculated to be the most stable, the $C_s$ structure has frequencies in better agreement with $CH_2D_2$ spectra suggesting that the two metal−hydrogen bonds are identical.

Like in the case of $CH_2=NbH_2$, the agostic distortion is even larger in configuration 2 (99.5° vs 85.0°), as shown in Figure 13, indicating along with previous results that the agostic distortion is a general phenomenon to stabilize the carbon−metal bond in high-oxidation-state complexes.[43,44] The Ta−H bonds are slightly shorter in configuration 1 than in configuration 2. The C=Ta bond length of 1.913 and 1.877 Å in configurations 1 and 2 are in the 1.87−2.09 Å range of bond lengths for large Ta alkylidene complexes.[1] The observed frequencies are compared with the predicted frequencies for configurations 1 and 2 in Table 8a,b, respectively.

**TABLE 13: Geometrical Parameters and Physical Constants of $CH_3-TaH$, $CH_2=TaH_2$, $CH\equiv TaH_3^-$, and $(CH_3)_2TaH_2$[a]**

| | | $CH_2=TaH_2$ | | | |
|---|---|---|---|---|---|
| parameters | $CH_3-TaH$ | config. 1 | config. 2 | $CH\equiv TaH_3^-$ | $(CH_3)_2TaH_2$ |
| $r$(C−Ta) | 2.150 | 1.913 | 1.877 | 1.822 | 2.146 |
| $r$(C−$H_1$) | 1.096 | 1.109 | 1.140 | 1.088 | 1.104 |
| $r$(C−$H_2$) | 1.096 | 1.083 | 1.079 | | 1.096 |
| $r$(Ta−$H_3$) | | 1.801 | 1.790 | 1.855 | |
| $r$(Ta−$H_4$) | 1.798 | 1.809 | 1.790 | 1.855 | 1.793 |
| $r$(Ta···$H_1$) | 2.766 | 2.365 | 2.109 | 2.910 | 2.607 |
| ∠$H_1CH_2$ | 108.9 | 114.2 | 113.7 | | 107.7 |
| ∠$H_2CH_3$ | 107.7 | | | | 108.9 |
| ∠$CtaH_3$ | | 111.1 | 102.2 | 104.3 | |
| ∠$CtaH_4$ | 120.4 | 121.6 | 102.2 | 104.3 | 110.6 |
| ∠$H_3TaH_4$ | | 124.3 | 115.9 | 114.1 | |
| ∠$H_1CTa$ | 112.8 | 99.5 | 85.0 | 180.0 | 101.8 |
| ∠$H_2CTa$ | 109.2 | 146.1 | 161.2 | | 115.0 |
| Φ($H_1CTaH_3$) | 121.2 | 10.9 | 119.9 | | 116.2 |
| Φ($H_1CTaH_4$) | 180.0 | 171.8 | −119.9 | | −116.2 |
| mol symm | $C_s$ | $C_1$ | $C_s$ | $C_{3v}$ | $C_{2v}$ |
| $q$(C)[b] | −0.28 | −0.59 | −0.61 | −0.82 | −0.72 |
| $q$(Ta)[b] | 0.58 | 1.16 | 1.12 | 1.19 | 1.89 |
| $q$($H_1$)[b] | −0.02 | 0.01 | −0.04 | 0.07 | 0.06 |
| $q$($H_2$)[b] | 0.00 | 0.05 | 0.06 | −0.48 | 0.02 |
| $q$($H_3$)[b] | 0.00 | −0.30 | −0.27 | −0.48 | 0.02 |
| $q$($H_4$)[b] | −0.29 | −0.33 | −0.27 | −0.48 | −0.32 |
| $\mu$[c] | 1.41 | 0.59 | 2.37 | 2.78 | 0.88 |
| state[d] | $^4A''$ | $^2A$ | $^2A'$ | $^1A_1$ | $^2A_2$ |
| $\Delta E$[e] | 20.6 | 29.2 | 27.2 | 70.8 (60.9[f]) | 58.5 |

[a] Bond lengths and angles are in Å and degree. Calculated at the level B3LYP/6-311++G(3df,3pd)/SDD. [b] Mulliken atomic charge. [c] Molecular dipole moment in D. [d] Electronic state. [e] Binding energies in kcal/mol relative to $CH_3F$ and Ta ($^6D$). [f] Binding energy in kcal/mol relative to $CH_3F$ and $^5Ta^-$ ($^5D$).

The **i** absorption at 1726.2 $cm^{-1}$ on the red side of the **m** hydrogen stretching absorptions also increases upon UV and full arc irradiation but decreases upon annealing, as shown in Figures 6−9. The $^{13}C$ substitution leads to a negligible shift, but deuteration leads to a shift of −489.4 $cm^{-1}$ (H/D isotopic shift of 1.396). We assign these absorptions of the isotopomers to the monohydrido insertion product, $CH_3-TaH$, following the case of Nb + $CH_4$. The predicted frequencies and intensities are compared with the observed values in Table 10. The metal−hydrogen stretching band is far stronger than the other modes, and the predicted frequencies for the isotopomers show a good agreement with the observed values. The calculated structure of $CH_3-TaH$ is shown in Figure 13, which is like $CH_3-VH$ and $CH_3-NbH$ structures in Figures 10 and 11. The predicted C−Ta bond length of 2.150 Å is longer and slightly shorter than those of 2.074 and 2.154 Å for $CH_3-VH$ and $CH_3-NbH$, respectively. The C−Ta bond length is also compared to that of 2.165 Å for $Cp'Ta(CHSiMe_3)(CH_2SiMe_3)_2$.[1]

A new absorption marked **a** is observed at 1567.8 $cm^{-1}$, substantially lower than the **m** absorption but still in the Ta−H stretching region, as shown in Figure 6, whereas two **a** absorptions emerge in the Ta−D stretching region, as shown in Figure 7, suggesting that the weak, high-frequency component of the Ta−H stretching absorption pair is overlapped by the stronger water residue absorptions. Two more diagnostic absorptions marked **a** are observed 917.6 and 574.6 $cm^{-1}$ in the Ta + $CH_4$ spectra. The $^{13}C$ and D substitutions give

frequency shifts of 0.1 and −441.2 $cm^{-1}$ (H/D isotopic ratio of 1.391) for the hydrogen stretching band at 1567.8 $cm^{-1}$. The absorption at 917.6 $cm^{-1}$ sustains shifts of −28.6 and −54.8 $cm^{-1}$ on $^{13}C$ and D substitution ($^{12}C/^{13}C$ and H/D ratios of 1.032 and 1.064), respectively. The large $^{13}C$ shift indicates the band originates from a vibrational mode including a large displacement of the carbon atom, and the frequency much higher than those expected for the C−Ta and C═Ta groups suggests that the band arises from the stretching mode of a carbon−metal triple bond (C≡Ta).

The **a** absorptions increase about 15% upon visible but decrease 60% on full arc irradiations, respectively. More importantly, they deplete completely on addition of a trace of $CBr_4$, which is very effective in removing electrons produced in the laser-ablation process,[26] which indicates that these absorptions belong to an anionic product of Ta + $CH_4$ reaction. On the basis of the observed vibrational frequencies, this anionic product is identified as the tantalum methylidyne trihydride anion complex ($CH{\equiv}TaH_3^-$) in line with the Nb case. The heavier group 5 transition metals form anionic alkylidyne complexes in reaction with methane, and the stability of the small carbyne complexes is based on the electronic structures of the metal anions being isoelectronic to those of group 6 transition-metal atoms, which are known to form various alkylidyne complexes.[1]

Figure 14 displays the relative energies of the plausible products relative to Ta($^4F_{3/2}$) + $CH_4$, where the most stable primary neutral products are $CH_3$−TaH and $CH_2{=}TaH_2$ in the quartet and doublet ground states, respectively. Clearly $CH{\equiv}TaH_3^-$ in its singlet ground state is the most stable reaction product among the plausible anionic products, parallel to the case with Nb. Figure 14 also shows that neutral $CH{\equiv}TaH_3$ formed by loss of an electron from $CH{\equiv}TaH_3^-$ is very unstable relative to more plausible neural products and probably ends up with formation of a more stable product. Therefore, the increase of $CH_2{=}TaH_2$ upon UV and full arc irradiations shown in Figures 6−8 results at least partly from the decrease of the anionic methylidyne complex, $CH{\equiv}TaH_3^-$, and Ta undergoes reactions analogous to (2) and (3).

Clearly the anion product of the Ta reaction with methane is more stable than the Nb counterpart, resulting in stronger anion product absorptions and allowing observation of the weaker low-frequency bands of the anionic species. This suggests that electron capture is more efficient in the Ta than in the Nb methylidene complex, reaction 3. Like the $CH{\equiv}NbH_3^-$ counterpart, $CH{\equiv}TaH_3^-$ has a $C_{3v}$ structure as shown in Figure 13. Previous studies report that the simple methylidyne trihydride complexes of group 6 transition metals also have $C_{3v}$ structures.[12,13] Due to the high bond order, the carbon−tantalum bond (1.822 Å) is shorter than those of $CH_3$−TaH (2.150 Å) and $CH_2{=}TaH_2$ (1.913 Å), but comparable to those of $CH{\equiv}NbH_3^-$ (1.797 Å) and $CH{\equiv}WH_3$ (1.742 Å). The C≡Ta bond length of the anionic complex is also compared to the C≡Ta bond length (1.849 Å) in Ta($\eta^5$-$C_5Me_5$)(CPh)($PMe_3$)$_2$Cl,[45] and to that calculated for the $CH{\equiv}TaH_3^-$ anion (1.80 Å) at the MC/LMO/CI level of theory.[21]

The absorptions marked **di** are observed at 1787.8 and 1761.4 $cm^{-1}$ on the blue side of the **m** absorptions in the Ta−H stretching region, as shown in Figures 6−9. They increase on photolysis (particularly UV and full arc) and in the early stage of annealing. More importantly, their relative intensities to the other sets of absorptions become much stronger at higher concentration of the precursor as shown in Figure 9, indicating that they arise from a high-order reaction product. The $^{13}C$ substitution leads to negligible shifts, whereas deuteration gives frequency shifts of −511.4 and −501.1 $cm^{-1}$ (H/D isotopic ratios of 1.400 and 1.398). In the Ta reaction with $CH_2D_2$, the single broad intermediate band at 1772 $cm^{-1}$ suggests a slight difference in the Ta−H bonds. These hydrogen stretching absorptions are assigned to a high-order reaction product, $(CH_3)_3TaH_2$, in line with the case of $(CH_3)_3NbH_2$.

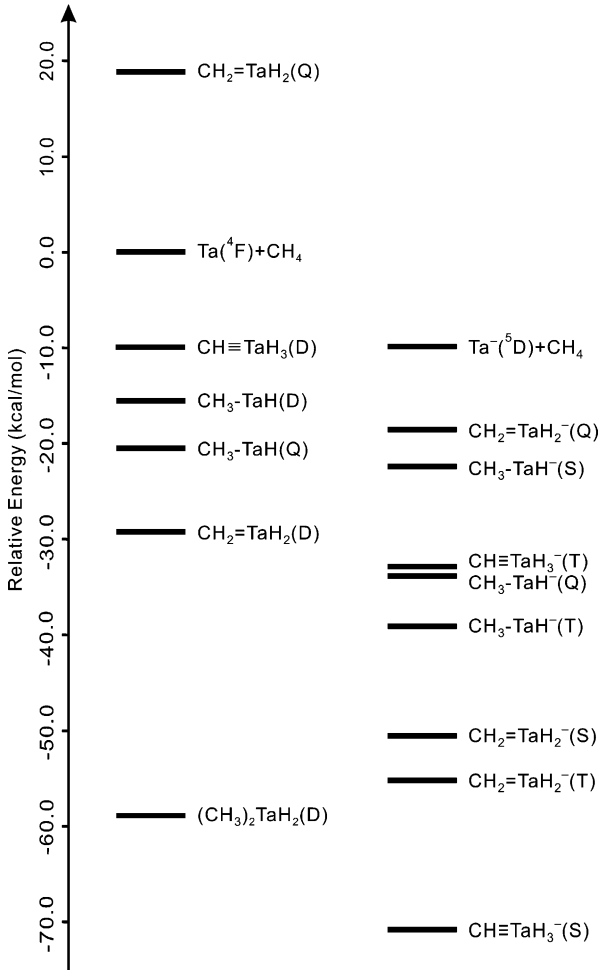


**Figure 14.** Energies of neutral and anionic products relative to Ta($^6D$) + $CH_4$. Note that $CH_3$−TaH(Q) and $CH_2{=}TaH_2$(D) are the most stable ones among the plausible neutral primary products. Formation of the high-order product, $(CH_3)_2TaH_2$(D), brings further stabilization. Also note that $CH{\equiv}TaH_3^-$(S) is the most stable one among the plausible anionic products. S, D, and Q denote singlet, doublet, and quartet states.

This confirms the fact that group 5 transition metals, similar to group 4 transition metals, form the dimethyl dihydride complexes $(CH_3)_2MH_2$, but the hydrogen stretching absorptions are much weaker with group 5 than with group 4.[1−8] On the other hand, no **di** absorptions are observed in the spectra from reaction of group 6 transition metals with methane or methyl halides in earlier studies.[12−15]

$(CH_3)_2TaH_2$ has a calculated $C_{2v}$ structure like the Nb counterpart, as shown in Figure 13, and the observed hydrogen stretching frequencies match well with the predicted values as shown in Table 11. The binding energy of $(CH_3)TaH_2$ is 29 and 38 kcal/mol larger than those of $CH_2{=}TaH_2$ and $CH_3$−TaH, respectively, and both of them are expected to form the high-order product. The methane activation energies for the methylidene dihydride complexes of group 4 transition metals are much higher than those of group 5 and 6 transition metals [$\Delta E$ = −37, −44, −51 kcal/mol for Ti, Zr, Hf are compared to −28 and −29 kcal/mol for Nb and Ta and −27 and −28

kcal/mol for Mo and W, respectively]. Kaupp predicted first the $C_{2v}$ structure of dimethyl titanium dichloride and argued that the influence of ligand-to-metal $\pi$-bond should be very important on the bond angles.[46] However, we have shown more recently that the bond angles of $(CH_3)_2TiF_2$ and $(CH_3)_2TiBr_2$ are very close to those of $(CH_3)_2TiCl_2$.[1−4]

**Group 4−6 Trends.** The results in the present and previous matrix isolation studies involving the reactions of groups 4−6 transition metal atoms with methane and methyl halides provide the following trends. On going down the column, high-oxidation-state complexes are more favored. The first row transition metals form the mono-insertion product ($CH_3MX$) primarily or even exclusively.[4,7,11,13,15] The high-oxidation-state complexes are mostly formed in the process of photolysis afterward (if formed).[4,7] On the other hand, the high-oxidation-state complexes as well as the mono-insertion products are formed by the second row transition metals. The high-oxidation-state products are even more favored by the third row transition metals, and in some cases, the mono-insertion products are not identified in the spectra.[6,10] This tendency is due to the fact that the high-oxidation-state complexes become more stable relative to the mono-insertion products on going down the column.

The neutral methylidyne complexes are produced only by group 6 transition metals in reactions with methane and methyl halides,[12−15] whereas the isoelectronic anionic methylidyne complexes are formed by group 5 transition metals. The group 5 transition-metal atom becomes isoelectronic to group 6 transition-metal atom in the same row by gaining one electron, and this suggests that the electronic structures of group 6 transition metals are essential to form the methylidyne complexes. On the other hand, the higher-order complexes ($(CH_3)_2MX_2$) are more readily formed by group 4 than group 5 transition metals,[4−11] whereas no evidence for the higher-order products of group 6 transition metals has been observed.[12−15] The high reactivity of group 4 transition metals to form the $(CH_3)_2MX_2$ probably originate at least partly from the large $\Delta E$'s of formation.

## Conclusions

Reactions of laser-ablated group 5 transition-metal atoms with methane in excess argon have been carried out during condensation at 8 K. Vanadium is very reactive with $CH_4$ and also selective in that only $CH_3-VH$ was observed. On the other hand, four sets of product absorptions (marked **m**, **i**, **a**, and **di**) were observed for each heavier metal on the basis of their spectroscopic characteristics and variations upon photolysis, annealing, and addition of a trace of $CCl_4$ or $CBr_4$. The **m** and **i** absorptions increase upon photolysis and decrease gradually upon annealing, and they are assigned to the primary neutral C−H insertion products, $CH_2{=}MH_2$ and $CH_3-MH$. The **a** absorptions decrease upon UV irradiation and more importantly, disappear completely upon addition of a trace of $CCl_4$ or $CBr_4$, which indicates anionic products. Thus, the methylidyne trihydride anion complexes, $CH{\equiv}MH_3^-$, are identified. The **di** absorptions are hardly discernible in the original spectrum but become more apparent in the process of photolysis and annealing, and they become relatively much stronger at higher concentration of the precursor. The **di** absorptions are assigned to a higher-order reaction products, $(CH_3)_3MH_2$. The assignments are confirmed by isotopic substitution and agreement with frequencies calculated using density functional theory.

The present results show that like group 4 and 6 transition metal atoms, the group 5 transition metal atoms readily form the C−H insertion products in reactions with methane. Group 5 transition-metal methylidyne systems are rare, and $CH{\equiv}NbH_3^-$ and $CH{\equiv}TaH_3^-$ are believed to be the first group 5 transition-metal methylidyne trihydride anion complexes. Calculations show that there are two stable configurations ($C_s$ and $C_1$) with similar energies for the doublet methylidene complexes, $CH_2{=}MH_2$, in both of which the $CH_2$ groups are distorted owing to agostic interaction. However, CCSD calculations suggest that multiconfiguration methods will be required to describe more accurately the molecular structures.

**Acknowledgment.** We gratefully acknowledge financial support from NSF Grant CHE 03-52487 to L.A.

## References and Notes

(1) Schrock, R. R. *Chem. Rev.* **2002**, *102*, 145.
(2) Schrock, R. R. *J. Am. Chem. Soc*. **1974**, *96*, 6796. **1975**, *97*, 6577.
(3) McLain, S. J.; Wood, C. D.; Messerle, L. W.; Schrock, R. R.; Hollander, F. J.; Youngs, W. J.; Churchill, M. R. *J. Am. Chem. Soc.* **1978**, *100*, 5962.
(4) Cho, H.-G.; Andrews, L. *J. Phys. Chem. A* **2004**, 108, 6294 (Ti + $CH_3F$).
(5) Cho, H.-G.; Andrews, L. *J. Am. Chem. Soc*. **2004**, *126*, 10485 (Zr + $CH_3F$).
(6) Cho, H.-G.; Andrews, L. *Organometallics* **2004**, *23*, 4357 (Hf + $CH_3F$).
(7) Cho, H.-G.; Andrews, L. *Inorg. Chem*. **2005**, *44*, 979 (Ti + $CH_3X$).
(8) Andrews, L.; Cho, H.-G.; Wang, X. *Angew. Chem., Int. Ed*. **2005**, *44*, 113 (Zr + $CH_4$).
(9) Cho, H.-G.; Wang, X.; Andrews, L. *J. Am. Chem. Soc*. **2005**, *127*, 465 (Zr + $CH_4$).
(10) Cho, H.-G.; Wang, X.; Andrews, L. *Organometallics* **2005**, *24*, 2854 (Hf + $CH_4$).
(11) Andrews, L.; Cho, H.-G.; Wang, X. *Inorg. Chem.* **2005**, *44*, 4834 (Ti + $CH_4$).
(12) Cho, H.-G.; Andrews, L. *J. Am. Chem. Soc*. **2005**, *127*, 8226 (Mo + $CH_4$).
(13) Cho, H.-G.; Andrews, L.; Marsden, C. *Inorg. Chem.* **2005**, *44*, 7634 (Cr, W + $CH_4$).
(14) Cho, H.-G.; Andrews, L. *Chem. Eur. J.* **2005**, *11*, 5017 (Mo + $CH_3F$).
(15) Cho, H.-G.; Andrews, L. *Organometallics* **2005**, *24*, 5678 (W + $CH_3F$).
(16) Tran, E.; Legzdins, P. *J. Am. Chem. Soc*. **1997**, *119*, 5071.
(17) Buchmeiser, M. R. *Chem. Rev*. **2000**, *100*, 1565.
(18) Cho, H.-G.; Andrews, L. *Organometallics* **2006**, *25*, 477.
(19) Franci, M. M.; Pietro, W. J.; Hout, R. F., Jr.; Hehre, W. J. *Organometallics* **1983**, *2*, 281, 815.
(20) Dobbs, K. D.; Hehre, W. J. *J. Am. Chem. Soc*. **1986**, *108*, 4663.
(21) Cundari, T. R.; Gordon, M. S. *J. Am. Chem. Soc*. **1992**, *114*, 539.
(22) Chung, G.; Gordon, M. S. *Organometallics* **2003**, *22*, 42.
(23) Duncalf, P. J.; Harrison, R. J.; McCamley, A.; Royan, B. W. *J. Chem. Soc., Chem. Commun.* **1995**, 2421.
(24) (a) Liu, X.; Li, L.; Diminnie, J. B.; Yap, G. P.A.; Rheingold, A. L.; Xue, Z. *Organometallics* **1998**, *17*, 4597. (b) Riley, P. N.; Thorn, M. G. Vilardo, J. S.; Lockwood, M. A.; Fanwick, P. E.; Rothwell, I. P. *Organometallics* **1999**, *18*, 3016.
(25) Zhou, M. F.; Andrews, L. *J. Phys. Chem. A* **1998**, *102*, 8251.
(26) Andrews, L.; Citra, A. *Chem. Rev*. **2002**, *102*, 885 and references therein.
(27) Wang, X.; Andrews, L. *J. Phys. Chem. A* **2003**, *107*, 570.
(28) (a) Frisch, M. J.; Trucks, G. W.; Schlegel, H. B.; Scuseria, G. E.; Robb, M. A.; Cheeseman, J. R.; Montgomery, J. A., Jr.; Vreven, T.; Kudin, K. N.; Burant, J. C.; Millam, J. M.; Iyengar, S. S.; Tomasi, J.; Barone, V.; Mennucci, B.; Cossi, M.; Scalmani, G.; Rega, N.; Petersson, G. A.; Nakatsuji, H.; Hada, M.; Ehara, M.; Toyota, K.; Fukuda, R.; Hasegawa, J.; Ishida, M.; Nakajima, T.; Honda, Y.; Kitao, O.; Nakai, H.; Klene, M.; Li, X.; Knox, J. E.; Hratchian, H. P.; Cross, J. B.; Adamo, C.; Jaramillo, J.; Gomperts, R.; Stratmann, R. E.; Yazyev, O.; Austin, A. J.; Cammi, R.; Pomelli, C.; Ochterski, J. W.; Ayala, P. Y.; Morokuma, K.; Voth, G. A.; Salvador, P.; Dannenberg, J. J.; Zakrzewski, V. G.; Dapprich, S.; Daniels, A. D.; Strain, M. C.; Farkas, O.;. Malick, D. K.; Rabuck, A. D.; Raghavachari, K.; Foresman, J. B.; Ortiz, J. V.; Cui, Q.; Baboul, A. G.; Clifford, S.; Cioslowski, J.; Stefanov, B. B.; Liu, G.; Liashenko, A.; Piskorz, P.; Komaromi, I.; Martin, R. L.; Fox, D. J.;.Keith, T.; Al-Laham, M. A.; Peng, C. Y.; Nanayakkara, A.; Challacombe, M.; Gill, P. M. W.; Johnson, B.; Chen, W.; Wong, M. W.; Gonzalez, C.; Pople, J. A. *Gaussian 03*, revision B.04; Gaussian, Inc.: Pittsburgh, PA, 2003 (see also references therein). (b) Stevens, P. J.; Devlin, F. J.; Chablowski, C. F.; Frisch, M. J.

*J. Phys. Chem*. **1994**, *98*, 11623. (c) Krishnan, R.; Binkley, J. S.; Seeger, R.; Pople, J. A. *J. Chem. Phys.* **1980**, *72*, 650. (d) Frisch, M. J.; Pople, J. A.; Binkley, J. S. *J. Chem. Phys.* **1984**, *80*, 3265. (e) Andrae, D.; Haussermann, U.; Daly, M.; Stoll, H.; Preuss, H. *Theor. Chim. Acta* **1990**, *88*, 123.

(29) Jacox, M. E. *J. Mol. Spectrosc.* **1977**, *66*, 272.

(30) (a) Van Zee, R. J.; Weltner, W., Jr. *J. Chem. Phys.* **1995**, *102*, 4367. (b) Wang, X.; Andrews, L. Unpublished data (Nb, Ta + $H_2$).

(31) Xiao, Z. L.: Hauge, R. H.; Margrave, J. L. *J. Phys. Chem*. **1991**, *95*, 2696.

(32) Aristov, N.; Armentrout, P. B. *J. Phys. Chem*. **1987**, *91*, 6178.

(33) De Vore, T. C. *J. Chem. Phys.* **1975**, *62*, 520.

(34) Vivanco, M.; Ruiz, J.; Floriani, C.; Chiesi-Villa, A.; Rizzoli, C. *Organometallics* **1993**, *12*, 1794 (V complex for C−V length).

(35) Green, D. W.; Gruen, D. M. *J. Chem. Phys.* **1972**, *57*, 4462.

(36) Lee, T. J.; Taylor, P. R.; Int. J. *Quantum Chem. Symp*. **1989**, *23*, 199.

(37) Billups, W. E.; Konarski, M. M.; Hauge, R. H.; Margrave, J. L. *J. Am. Chem. Soc*. **1980**, *102*, 7394.

(38) Klabunde, K. J.; Jeong, G. H.; Olsen, A. W. In *Selective Hydrocarbon Activation: Principles and Progress*; Davies, J. A, Watson, P. L., Greenberg, A., Liebman, J. F., Eds.; VCH Publishers: New York, 1990; pp 433−466.

(39) Bloomberg, M. R. A.; Siegbahn, P. E. M.; Swensson, M. *J. Am. Chem. Soc*. **1992**, *114*, 6095.

(40) Jaffart. J.; Etienne, M.; Maseras, F.; McGrady, J. E.; Eisenstein, O. *J. Am. Chem. Soc*. **2001**, *123*, 6000.

(41) Pyykko, P. *Chem. Rev*. **1988**, *88*, 563.

(42) Graham, W. R. M.; Weltner, W., Jr. *J. Chem. Phys.* **1972**, *56*, 4400 (Ta absorption).

(43) Ujaque, G.; Cooper, A. C.; Maseras, F.; Eisenstein, O.; Caulton, K. G. *J. Am. Chem. Soc*. **1998**, *120*, 361.

(44) Scherer, W.; McGrady, G. S. *Angew. Chem., Int. Ed.* **2004**, *43*, 1782.

(45) McLain, S. J.; Wood, C. D.; Messerle, L. W.; Schrock, R. R. *J. Am. Chem. Soc*. **1978**, *100*, 5962 (C≡Ta bond length).

(46) Kaupp, M. *Chem. Eur. J*. **1999**, 5, 3631.